Annales Societatis Geologorum Poloniae (2007), vol. 77: 39–67.

ENVIRONMENTAL CHANGES AROUND THE CENOMANIAN–TURONIAN BOUNDARY IN A MARGINAL PART OF THE OUTER CARPATHIAN BASIN EXPRESSED BY MICROFACIES, MICROFOSSILS AND CHEMICAL RECORDS IN THE SKOLE NAPPE (POLAND)

Krzysztof BĄK

Institute of Geography, Pedagogical University, Podchorążych 2, 30-084 Kraków, Poland; e-mail: sgbak@cyf-kr.edu.pl

Bąk, K., 2007. Environmental changes around the Cenomanian–Turonian boundary in a marginal part of the Outer Carpathian Basin expressed by microfacies, microfossils and chemical records in the Skole Nappe (Poland). *Annales Societatis Geologorum Poloniae*, 77: 39–67.

Abstract: Lithology, microfacies, benthic foraminiferal and bulk chemical analyses of the Spława section in the Skole Nappe, Outer Carpathians (Poland) reflect environmental changes across the Cenomanian–Turonian transition. Biogenic-rich-turbidite sedimentation preceded the organic-rich sedimentation in the Skole Basin, terminating in the latest Cenomanian in response to progressive eustatic sea-level rise and to expansion of an oxygen minimum zone. The uppermost Cenomanian black, laminated, organic-rich shale series records the oceanic anoxic event (OAE-2). The benthos-free black non-calcareous shales exhibiting positive excursions of chemical redox indexes are indicative of bottom-water anoxia, interrupted by periods of suboxic conditions with sedimentation of hemipelagic green shales with poor agglutinated foraminiferal assemblages. An extremely low sedimentation rate or even a hiatus and an increase in deep-water circulation causing basin oxygenation resulted in precipitation of a ferromanganese layers and siliceous-manganiferrous variegated shales, as documented by low values of chemical redox indices. However, the lack of benthos and bioturbation, and low values of the Ce/La ratio in the subsequent succession of variegated shales (dominated by green shales) indicate a return to stressed conditions at basin floor with sluggish bottom water circulation, which occasionally resulted in sea floor anoxia with deposition of organic-rich shales. The long-termed well-oxygenated conditions at the basin floor appeared in the Early Turonian, as documented by diversified benthic foraminiferal assemblages. The frequency of radiolarian-rich layers and Ba/Al and Ba/Sc ratios increase up-section, reflecting an increase in primary productivity, induced by upwelling circulation.

Keywords: Cenomanian–Turonian boundary event, microfacies, benthic foraminifers, bulk geochemistry, Outer Carpathians, Poland.

Manuscript received 19 October 2006, accepted 29 March 2007

INTRODUCTION

In the deep-water environment, the Cenomanian–Turonian boundary interval is globally marked by the presence of organic-carbon-rich black shales, associated with radiolarian-rich layers. Since the 1970, this interval, originally termed the Cenomanian–Turonian Anoxic Event (OAE; Schlanger & Jenkyns, 1976), and later referred to as the Bonarelli Event, the OAE-2, and the Cenomanian–Turonian Boundary Event (CTBE), has become one of the most studied Phanerozoic oceanic events. Despite existence of many contributions related to the OAE-2 (e.g., Arthur, 1979; Jenkyns, 1980; Summerhayes, 1981; Arthur & Premoli Silva, 1982; Bralower & Thierstein, 1984; Herbin *et al.*, 1986; Kuhnt *et al.*, 1990; Pedersen & Calvert, 1990; Peryt & Wyrwicka, 1991, 1993; Tyson, 1995; Sinninghe Damsté & Köster, 1998; Gustafsson *et al.*, 2003; Lüning *et al*, 2004; Kuhnt *et al.*, 2005; Wójcik-Tobol, 2006), little is known about its record from basins with sedimentation below the CCD. The record of OAE-2 from such deep-water environment comes mainly from the trench basins located close to the margins of the Western Tethys and the North Atlantic DSDP/ODP sites (Sites 398, 641A; Herbin *et al.*, 1986, 1988; Kuhnt *et al.*, 1990). In the Mediterranean part of the Tethys, the Cenomanian–Turonian boundary (CTB) deep-water organic-rich facies were recorded from the

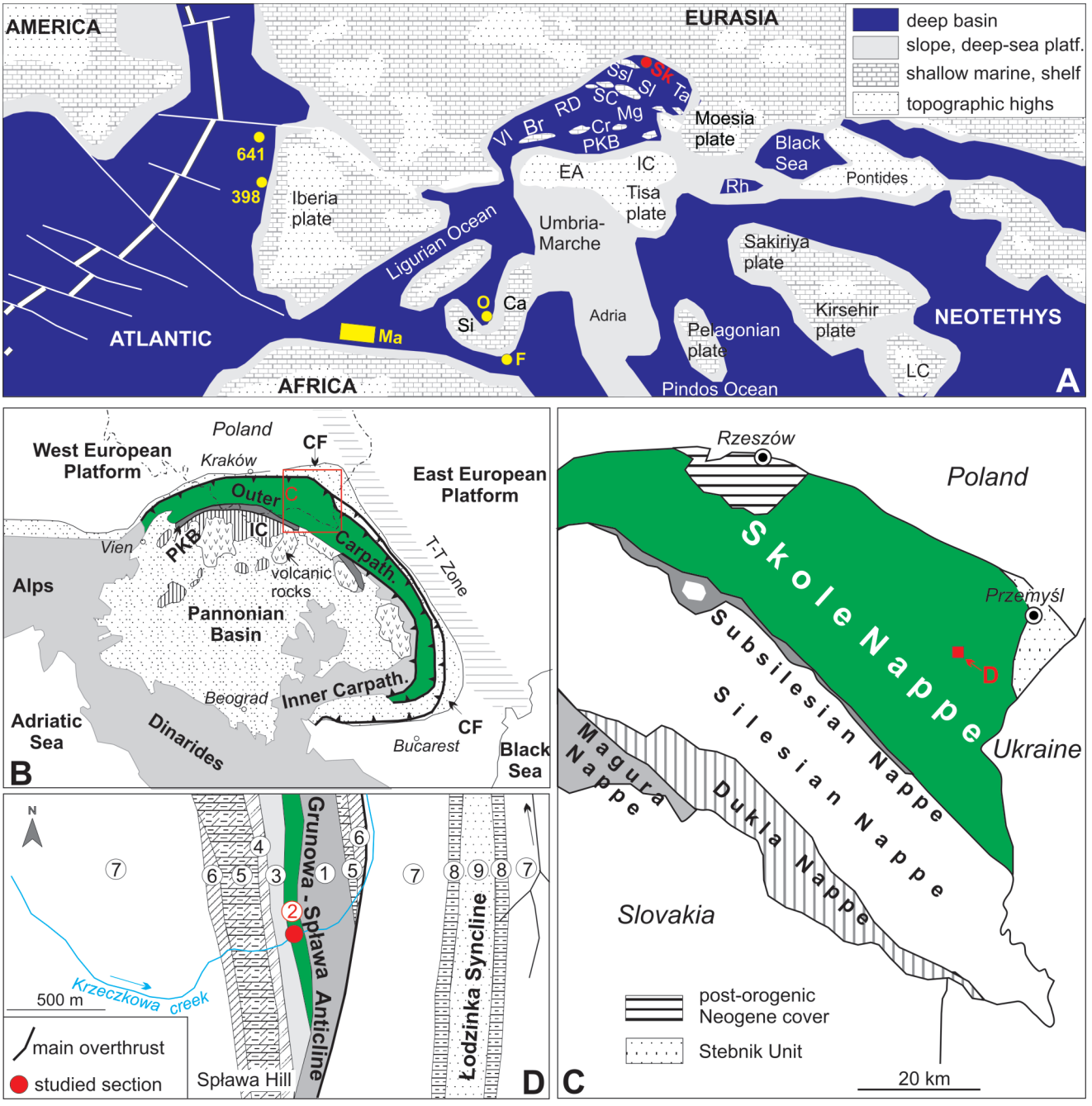

Fig. 1. **A** – Palaeogeographical map of the Western Tethys across the Carpathians during the Turonian (90 Ma) (after Golonka *et al.*, 2000; Golonka & Krobicki, 2001; simplified) showing the position of the studied section in the Skole Basin (Sk), and the lower bathyal–abyssal sites (below the CCD) with organic-rich deposition in the marginal parts of the eastern North Atlantic (Sites 398 and 641) and the Western Tethys (F – Floresta section, O – Oriolo section; Ma – Mauretanian – Massylian flysch nappes). Abbreviations of ocean and plate names: Br – Briançonnais terrane, Ca – Calabria-Campania terrane, Cr – Czorsztyn Ridge, EA – Eastern Alps, IC – Inner Carpathians, LC – Lesser Caucasus terrane, Mg – Magura Basin, PKB – Pieniny Klippen Belt Basin, RD – Rheno-Danubian Basin, Rh – Rhodopes, SC – Silesian Ridge (Cordillera), Si – Sicily plate, Ssl – Silesian Basin, SSl – Subsilesian Submerged Ridge, Ta – Tarcau Basin, Vl – Valais trough. **B** – Outer Carpathians against the background of a simplified geological map of the Alpine orogens and their foreland; IC – Inner Carpathians, CF – Carpathian Foredeep, PKB – Pieniny Klippen Belt. **C** – Skole Nappe against the background of the eastern part of the Polish Outer Carpathians. **D** – Geological map of the Skole Nappe around the Grunowa – Spława Anticline, with position of the studied section (after Gucik, 1987; simplified); 1 – Spas Shales (Barremian–Albian); 2 – Barnasiówka Radiolarian Shale Formation (?Middle Cenomanian–lowermost Turonian); 3 – siliceous marls with shale, and sandstone intercalations (Turonian); 4 – variegated shales from Kanasin (Turonian); 5 – marls with shale and sandstone intercalations (Turonian–Campanian); 6 – variegated and grey marly shales (Coniacian–Campanian); 7 – sandstones and shales with intercalations of variegated shales (undivided: Turonian–Paleocene); 8 – variegated shales (Lower Eocene); 9 – shales and thin-bedded sandstones of Hieroglyphic beds (Lower–Middle Eocene)

Mauretanian and Massylian nappes (Herbin *et al.*, 1986), the Calabrian Arch (Oriolo section; Kuhnt *et al.*, 1990) and SE Sicily (Floresta section; Kuhnt *et al.*, 1990), and also from the Outer Carpathians (Fig. 1). K. Bąk (2006, 2007a) made detailed biostratigraphic, sedimentological and chemical investigations of sections from the Subsilesian and Silesian nappes, corresponding to the deep submerdged ridge and marginal basin, respectively.

This paper presents facies evolution and the observed lithological, micropalaeontological (benthic foraminiferal) and chemical changes across the CTB in the Skole Basin, another marginal basin of the Outer Carpathians, located northeast of the Subsilesian Submerged Ridge, close to the southern margin of the European Platform (Fig. 1A). The investigations are based on data from various facies, exposed at the Spława section, in the central part of the Skole Nappe, Poland (Fig. 1C). The main objective of this study is to provide a detailed microfacies and chemical record of the CTB succession to explain the changes: 1) in oxygen content in the bottom water, 2) in palaeoproductivity, and 3) in sources of biogenic and terrigenous material supplied to the basin floor. All these changes are correlated with the critical $\delta^{13}C$ isotope excursion and biostratigraphic data recorded from this section during earlier studies (Bąk K., 2007b).

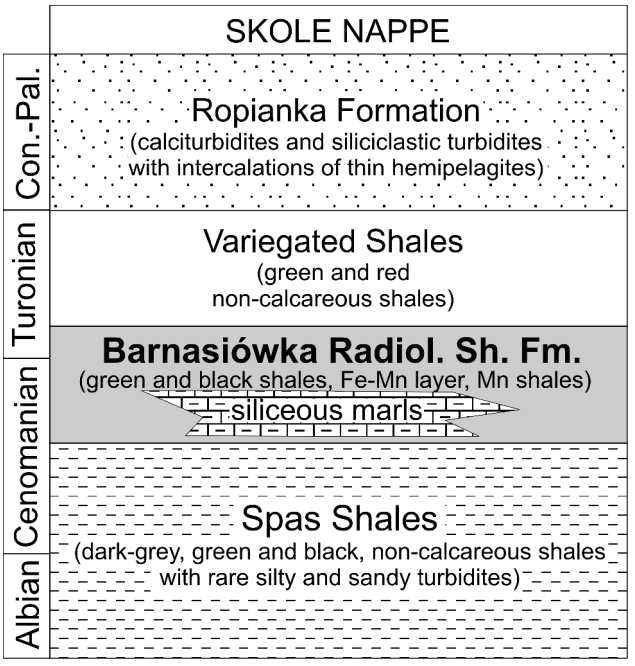

Fig. 2. Lithostratigraphy of the Albian–Paleocene deposits in the Skole Nappe, Polish Outer Carpathians (after Koszarski & Ślączka, 1973; supplemented)

REGIONAL SETTING

The Skole Nappe, exposed along the northern margin of the Outer Carpathians within the Polish and Ukrainian territories (Fig. 1B, C), comprises up to 3.8 km thick series of Barremian–Lower Miocene flysch sediments (Poprawa & Nemčok, 1998) deposited in an independent sedimentary area of the Outer Carpathians (cf. Książkiewicz, 1962; Oszczypko, 2004), the Skole Basin (Fig. 1A). The mid-Cretaceous sediments of the Skole Nappe are represented by silty and clayey turbidites (the Bełwin Mudstones and Spas Shales), with sandy turbidite intercalations (the Kuźmina Sandstones), which pass into the green radiolarian and black shales including silicified marls (the Barnasiówka Radiolarian Shale Formation; Fig. 2). The latter sediments, which are the subject of the present study, come from the Cenomanian–Turonian transition interval (Bąk K. *et al.*, 2001). They are followed by the Variegated Shales and the subsequent succession of calciturbidites and siliciclastic turbidites (the Ropianka Formation; Kotlarczyk, 1978).

Lithostratigraphy and geological section

The Cenomanian–Turonian sediments were earlier mapped in various zones of the Skole Nappe. These sediments occur in its northern marginal part (Zawada near Tarnów – Koszarski & Morgiel, 1963; Niedźwiada near Dębica – Gucwa, 1966; Szczepanowice near Wojnicz – Ślączka & Kaminski, 1998) and in the inner part, in both, the Polish (Rybotycze and Spława localities; Kotlarczyk, 1978; Gucik, 1987; Gucik *et al.*, 1991) and Ukrainian Carpathians (Skole skiba and Paraszka skiba in the Stryj and Dniestr valleys – Sujkowski, 1932; Zhurakovsky, 1968).

The above mentioned Cenomanian–Turonian sediments of the Skole Nappe have been distinguished as informal units, under a variety of names, and in a varied lithostratigraphic sense. The descriptions and correlations of the earlier described sections have been summarized by Bąk K. *et al.* (2001). Following this discussion, the studied sediments are included in the Barnasiówka Radiolarian Shale Formation (BRSF; Fig. 2), a unit which includes the Upper Cenomanian–Lower Turonian sediments, also of the Silesian and Subsilesian nappes. These sediments represent the middle and upper parts of the formation, being underlain by variegated non-calcareous shales. Locally, the silicified marl series occurs within the middle part of this formation (Fig. 2). These marls were earlier recorded from various localities of the Skole Nappe (Kotlarczyk, 1978; Gucik, 1987; Gucik *et al.*, 1991).

The studied section, named here as the Spława section, is located in the inner part of the Skole Nappe (in Poland), within the Grunowa – Spława Anticline, on both banks of the Krzeczkowa creek, north of the Spława Hill, about 25 km SW of Przemyśl (Fig. 1C, D). In this area, the BRSF is represented by (Fig. 3): 1) green non-calcareous shales (a dozen metres thick; not studied here), 2) thin-bedded siliceous marls with intercalations of green, grey and black shales (at least 20 m thick), 3) organic-rich series with bentonites and a ferromanganese layer at the top (1.7 m thick), 4) and variegated siliceous-manganiferous shales with the second ferromanganese layer and a thin organic-rich shale

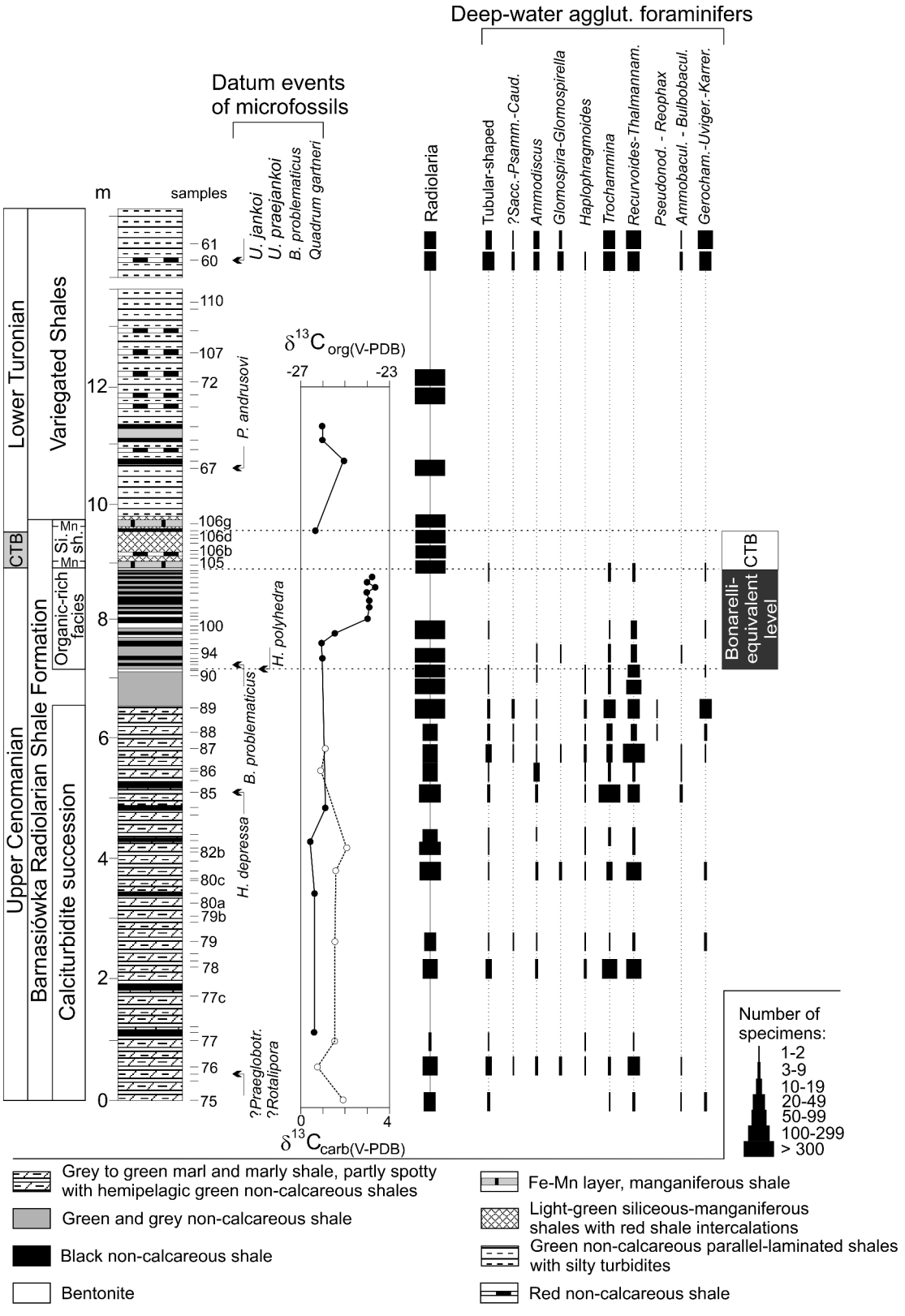

Fig. 3. Lithological log of the Spława section (Skole Nappe, Outer Carpathians) plotted against main microfossil and chemostratigraphic events (microfossils after Bąk K. *et al.*, 2005, Bąk K., 2007b); Si sh. – siliceous-manganiferous shales; Mn – ferromanganese layer

(0.7 m thick). The subsequent succession of Variegated Shales, overlying the BRSF, occurs in two packages (4.0 m and 1.2 m thick); the second one creates a thin tectonic slice (Fig. 3).

UPPER CENOMANIAN–LOWER TURONIAN STRATIGRAPHY

The base of the Turonian was assigned to the lowest occurrence (FO) of the ammonite *Watinoceras devonense* Wright & Kennedy, which is close to the end of the OAE-2 (for summary – see Bengston, 1996; Gradstein *et al.*, 2004). Below the boundary lies the highest occurrence of the planktonic foraminifer *Rotalipora*. Above the boundary are the lowest occurrences of the planktonic foraminifer *Helvetoglobotruncana helvetica*, and the calcareous nannoplankton *Quadrum gartneri* (Gradstein *et al.*, 2004). Among the siliceous microfauna, the radiolarian species *Alievum superbum* and *Crucella cachiensis* are regarded as taxa that appeared close to the C–T boundary (Bąk M., 2000, 2004). Unfortunately, the datum events of calcareous microfossils can be diachronous due to ecological effects (Paul *et al.*, 1999; Luciani & Cobianchi, 1999; Leckie *et al.*, 2002; Erba, 2004; Kuhnt *et al.*, 2005; Caron *et al.*, 2006), and the only tool for stratigraphy of the deep-water sections across the CTB is a correlation with a global positive excursion in the carbon-13 isotope. In the stratotype section at Pueblo, the FO of *W. devonense* lies close to the maximum peak of $\delta^{13}C$ that terminates the $\delta^{13}C$ plateau (Pratt & Threlked, 1984; Keller *et al.*, 2004; Tsikos *et al.*, 2004; Sageman *et al.*, 2006; Caron *et al.*, 2006).

Foraminiferal and radiolarian datum events presented by K. Bąk (2007b) from the Spława section show that the calciturbidite series (perhaps except for the base of the section) and the organic-rich facies represent the time period after extinction of *Rotalipora* morphotypes (lower part of foraminiferal *Whiteinella archaeocretacea* Zone; Fig. 3). In turn, the chemostratigraphic data show that the deposition of organic-rich facies began close to the beginning of the $\delta^{13}C$ rise (Fig. 3). Following the correlation of geochemical datum lines with the CTB section in the Silesian Nappe, and its calibration with the stratotype section at Pueblo (Colorado), this first initial rise in $\delta^{13}C$ values took place ca. 430 kyr before the C–T boundary, based on the orbital time scale of Sageman *et al.* (2006; for details – see Bąk K., 2007a). The end of organic-rich sedimentation corresponds to a plateau interval (?its termination), after the second maximum in $\delta^{13}C$ values within the excursion interval (Fig. 3). Probably, it took place close to the CTB, *i.e.* ca 30–50 kyr before the boundary (Bąk K., 2007b). The precipitation of the first Fe-Mn layer and the overlying siliceous-manganiferous shales terminated close to the CTB, as suggested by a low $\delta^{13}C$ value of the next organic-rich shale, present directly below the second Fe-Mn layer. This datum marks the recovery interval of the $\delta^{13}C$ values, which began ca. 300 kyr after the CTB, taking into account the comparison with the orbital time scale of Sageman *et al.* (2006). It suggests that precipitation of the Fe-Mn layer and the 60-cm-thick siliceous-manganiferous shales lasted at least 330–350 kyr. The precise age determination of the younger sediments, *i.e.* the second level of the Fe-Mn sediments and the overlying variegated shales, is impossible. This part of the section represents the ?Lower Turonian, based on the occurrence of the benthic foraminifer *Uvigerinammina jankoi* and calcareous nannoplankton species *Quadrum gartneri* (Gaździcka in: Bąk K. *et al.*, 2005). Both taxa occur in the topmost package of the variegated shales.

MATERIAL AND METHODS

The Spława section is represented by 79 samples collected from a nearly 15 m thick succession. Microfossils (foraminifers and radiolarians) have been extracted from 47 samples, of 200–300 g, which were dried and dissociated by repeated heating and drying in a sodium carbonate solution (ten samples were barren of microfossils). Additionally, microfossil components were determined in 46 thin sections of resistant siliceous shales and marls.

The main components from 45 samples of sediments were determined by inductively coupled plasma–optical emission spectrometry (ICP–OES); trace elements, including rare earth elements (REE), were determined by inductively coupled plasma mass spectrometry using a Thermo Instruments PQII ICP-MS at the Activation Laboratories Ltd in Lancaster, Canada. Electron microprobe point analyses of selected mineral constituents of the hemipelagic shales were carried out using a Hitachi S-4700 SEM with a link Noran Vantage EDS (electron beam focused on 1 μm with 20-25 kV accelerating voltage; counts acquired for 150 seconds; the data were corrected using the ZAF/PB programme) at the Institute of Geological Sciences, Jagiellonian University, Kraków.

RESULTS

Microfacies and microfossils

The studied part of the BRSF, 9.7 m thick, consists of a succession of 1) siliceous marls (calciturbidites) with intercalations of hemipelagic non-calcareous green, grey and black shales, 2) black, green, grey and blue clayey shales (organic-rich facies), 3) first ferromanganese layer, and 4) green, siliceous-manganiferous shales with thin red shale intercalations, and the second level of the Fe-Mn layer at the top (Fig. 3). This formation is overlain by Variegated Shales (non-calcareous, clayey at the top), with rare and thin intercalations of black shales. This unit occurs in two packages, which are in tectonic contact.

Calciturbidite series

Light-green, siliceous, thin- to medium-bedded marls and marly shales with intercalations of green, non-calcareous shales, and a few black, organic-rich shales represents

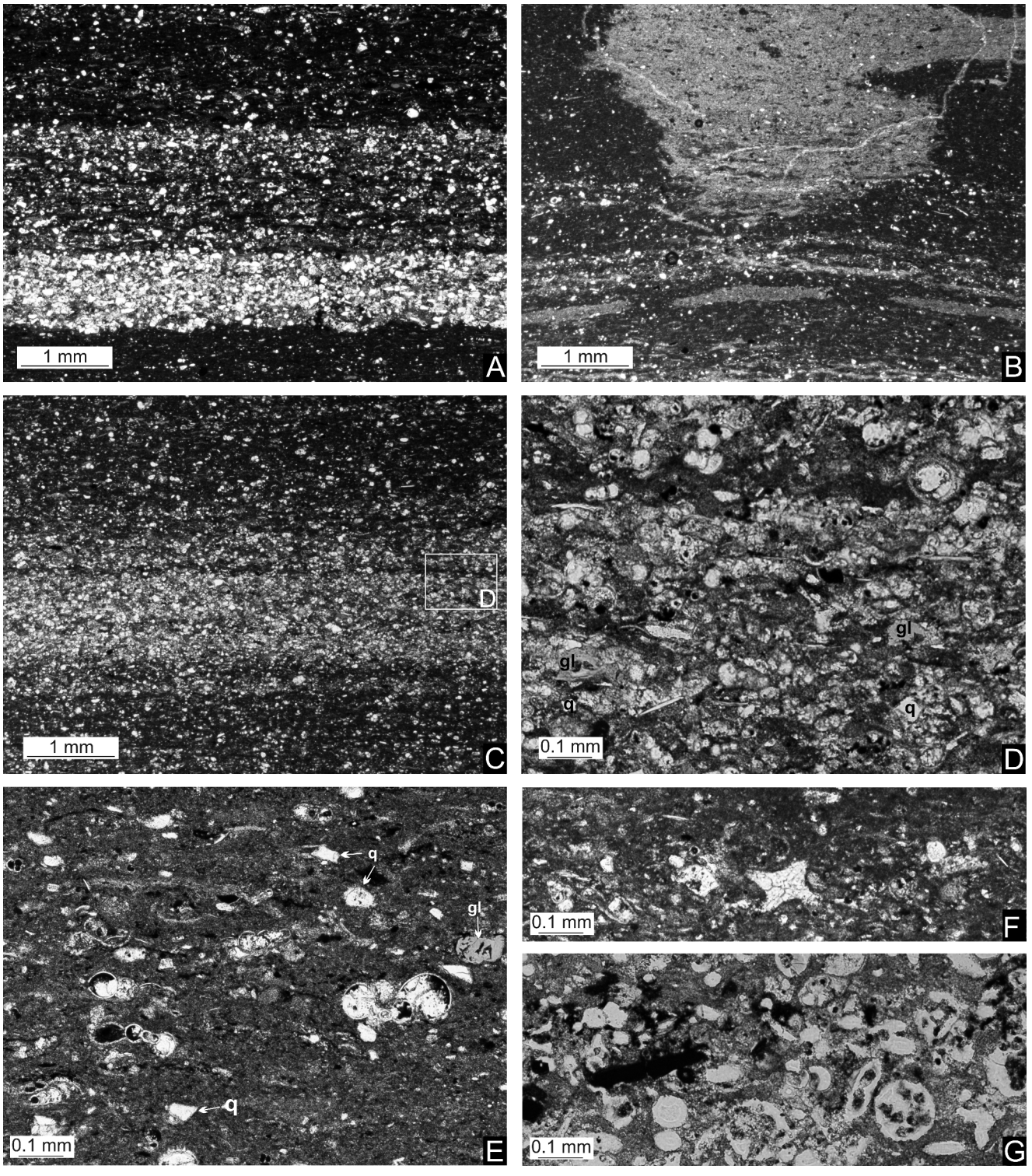

Fig. 4. Microfacies of the Upper Cenomanian calciturbidite series. **A** – Parallel-laminated packstone passing to foraminiferal wackstone (sample Krz-75b); **B** – *Chondrites* ichsp. traces in foraminiferal grainstone (Krz-77c); **C, D** – Foraminiferal-rich packstones that form laminae in hard marl layer (Krz-82b); **E** – Planktonic foraminiferal grainstone, dominated by specimens of *Hedbergella* and *Globigerinelloides* with admixture of quartz (q) and glauconite (gl) grains (Krz-89c); **F** – Sponge spicules in foraminiferal grainstone (Krz-79b); **G** – Radiolarian grainstone; note the calcareous matrix of the sediment (Krz-80c)

a lower part of the studied section, 6.5 m thick (Fig. 3). The marls occur in layers, from 2 to 25 cm thick (4–6 cm on average). Microfacies of the marls show that their bedding is related to diagenetic changes rather than to synsedimentary structures. The marls contain very thin layers (2–20 mm thick) of calciturbidites (Fig. 4A–C). Most of them are parallel-laminated silty layers (grainstones), built of quartz, calcite, glauconite and numerous fragmented foraminiferal tests, and sponge spicules (Fig. 4D). They pass into calcareous clays (wackstones) with fragmented foraminiferal tests, mainly planktonic (Fig. 4E). The proportion of terrigenous to biogenic particles changes in turbidite layers along the section, although most (ca. 90%) of the very-fine grained sandy and silty laminae are dominated by biogenic particles, mainly planktonic foraminifers. The planktonic foraminifers are represented by small-sized forms of *Hedbergella*, *Globigerinelloides*, *Heterohelix* and ?*Whiteinella* (Fig. 5A–D); only a few poorly-preserved "keeled" specimens of ?*Praeglobotruncana*, ?*Rotalipora* (Fig. 5E) have been recognized at the base of the section. Some layers of calciturbidites are fine-grained packstones, which consist of calcareous grains with numerous benthic and planktonic foraminifers, and partly radiolarians and sponge spicules (Fig. 4F). Well-preserved benthic foraminifers belong to the calcareous forms, dominated by specimens of gavelinelids (Fig. 5F–J), *Gyroidinoides* (Fig. 5K, L), *Lenticulina* (Fig.5M, N, R), ?*Nodosaria* (Fig. 5O), and *Dentalina* (Fig. 5P).

Higher up in the section, foraminiferal-spiculitic grainstones passing to wackstones are richer in radiolarians (Fig. 4G). These occur in separate laminae or are mixed with sponge spicules (Fig. 5S). Radiolarians occur as moulds, where microcrystalline quartz has replaced the opaline silica from skeletons, and CT-opal has infilled the skeletons. The radiolarians are poorly diversified, dominated by spherical specimens of the genus ?*Holocryptocanium* (Figs 4G, 5S). The sponge spicules belong to the hexactinellids (Fig. 6B–D) and demosponges (Fig. 6A, E–M). They occur mainly in the grainstone and packstone layers, but they are also found in the calcareous shales. The spicules occurring together with calcareous benthic foraminifers in the packstone and grainstone layers are calcified, while those from the shales have not been diagenetically altered. Many of the calciturbidites include small traces of *Chondrites* ichnsp. (Fig. 4B) and *Thalassinoides* ichnsp.

All calciturbidite layers, except for the fine-grained sandy packstones, are strongly impregnated with recrystallized silica. Foraminiferal tests are filled with microcrystalline quartz. The foraminifers from the marl beds in the highest part of this succession are additionally impregnated with ferromanganese oxyhydroxides, which have replaced the calcite from the test walls.

The green marly shales passing to hemipelagic non-calcareous shales occur as very thin intercalations among the calciturbidites. Some of them are enriched in organic matter. The green non-calcareous shales include small (< 0.05 mm), angular grains of detrital quartz and micas. Deep-water agglutinated foraminifers (DWAF), including siliceous and organic-walled forms, dominate the microfauna of these hemipelagic shales. They are represented mainly by *Plectorecurvoides* sp. (Fig. 7T), *Recurvoides* sp. (Fig. 7U), *Thalmannammina* spp. (Fig. 7S, V), *Glomospira charoides* (Fig. 7G), *Ammodiscus cretaceus* (Fig. 7F), *Bulbobaculites problematicus* (Fig. 7L), *Gerochammina* spp. (Fig. 7W, Z), and *Trochammina* sp. (Fig. 7N, O). Additionally, there have been found rare specimens of tubular forms (Fig. 7A, B), associated with *Pseudonodosinella parvula* (Fig. 7K), *Hippocrepina depressa* (Fig 7C), *Psammosphaera* sp. (Fig. 7D), *Caudammina ovula* (7E), and *Haplophragmoides* spp. (Fig. 7P, R).

Organic-rich facies

The calciturbidite sediments pass gradually to hemipelagic organic-rich facies (6.5–7.2 m from base of the section). This facies (7.2–8.9 m from base of the section) consists of green, radiolarian-rich and organic-rich layers, a few cm thick, with a relatively high TOC content, from 3.2% to nearly 8% in the studied samples (Bąk K., 2007b).

Poorly-preserved radiolarians (pyritized or as quartz moulds) dominate the microfossils of this series. Of the foraminifers, only poorly-preserved, small-sized DWAF have been determined there (Fig. 3), including mainly *Recurvoides* sp., and single specimens of *Ammodiscus cretaceus*, *Glomospira gordialis* (Fig. 7H), *Glomospirella gaultina* (Fig. 7I); *Haplophragmoides* sp., *Gerochammina* sp., ?*Saccammina* sp., *Trochammina* sp. (Fig. 7M), and pyritized tube-shaped forms. The abundance of benthic foraminifers does not exceed 10 specimens per 100 g of sediment.

Some green shale layers include a small number of redeposited sponge spicules. This series also contains of three 0.5–12 cm bentonites. Angular grains of quartz, feldspar, glauconite and micas, and single well-rounded grains of quartz are subordinate components in these sediments; all grains are less than 0.1 mm in diameter.

First ferromanganese layer

The ferromanganese layer, 1.5–3 cm thick, occurs 8–10 cm above the top of the organic-rich facies (Fig. 3), lying directly on the green shale, that is underlined by a thin bentonite. The Fe-Mn layer is made of concentrically zoned microspherules and pseudomorphs after rhombohedric crystals of carbonates, occurring within a matrix of collomorphic silica, microcrystalline quartz, clay minerals, and terrigenous muscovite (Bąk K. 2007b). The microspherules and pseudomorphs are made of collomorphic and microcrystalline barium manganese oxides, and ferromanganese oxyhydroxides. The internal structure and composition of the Fe-Mn layer is similar to the Fe-Mn horizon in the Subsilesian and Silesian nappes, lying in the same stratigraphic position (Bąk K., 2006, 2007a, b).

Siliceous-manganiferous shales with the second Fe-Mn layer

The siliceous-manganiferous shales, 70 cm thick, consist of green, radiolarian-rich non-calcareous shales with intercalations of red shales. They contain Fe-Mn oxide-hydro-

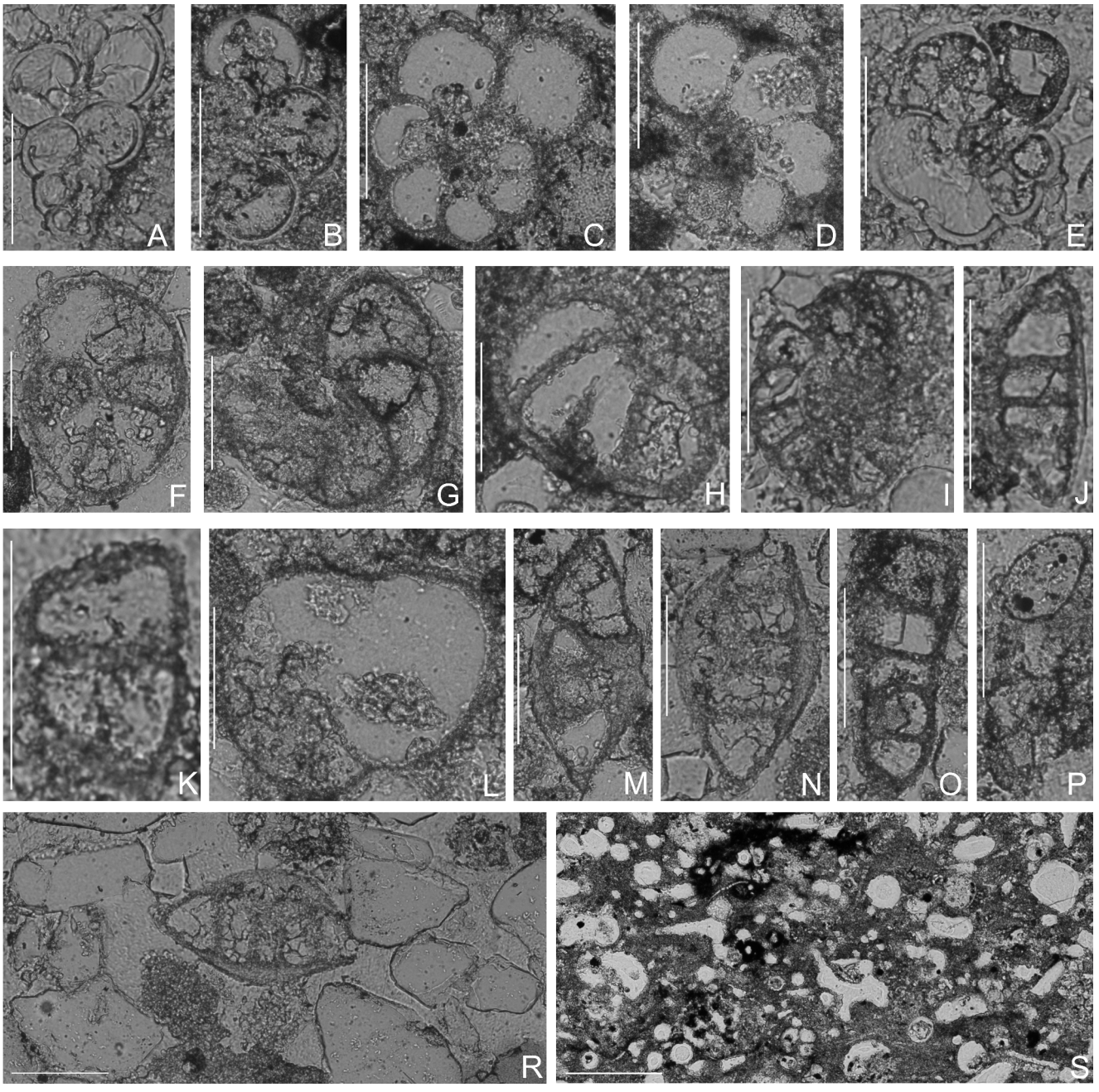

Fig. 5. Planktonic and benthic foraminifers (A–P) from the Upper Cenomanian calciturbidite series: **A** – *Heterohelix* sp. (sample Krz-75b); **B** – *Hedbergella* sp. (Krz-80c); **C, D** – *Globigerinelloides* sp. (Krz-80c); **E** – ?*Praeglobotruncana* (?*Rotalipora*) sp. (Krz-75b); **F**–**J** – gavelinelids (F–H – Krz-80c; I, J – Krz-75b); **K, L** – *Gyroidinoides* sp. (K – Krz-75b; L – Krz-80c); **M, N** – *Lenticulina* sp. (Krz-80c); **O** – ?*Nodosaria* sp. (Krz-75b); **P** – *Dentalina* sp. (Krz-75b); **R** – *Lenticulina* sp. within detritic calcareous grains (Krz-80c); **S** – Radiolarians and sponge spicules in calcareous matrix (Krz-80c). Length of scale bar – 100 μm

xides, filling up cracks, and occurring as encrustations (Fig. 8K–M). The first red shale laminae (enriched in radiolarians), 1–2 mm thick, appear 5 cm above the Fe-Mn layer. A green shale layer which divides these red laminae contains numerous small-sized, conical-shaped agglutinated foraminifers belonging to *Gaudryina* sp. or *Uvigerinammina* sp., and also to ?*Ammodiscus* sp. The overlying sediments are completely devoid of foraminifers. DWAF assemblages do not occur earlier up-section than the second package of non-calcareous variegated shales (Fig. 3).

Radiolarians, as the only biotic component occurring in the remaining part of the siliceous-manganiferous shales (Fig. 8C–J), create 1–3 mm thick laminae which are hemipelagic deposits (Fig. 8A); some of these laminae could be reworked sediment, as is shown by densely-packed skeletons of similar dimensions (Fig. 8B, K).

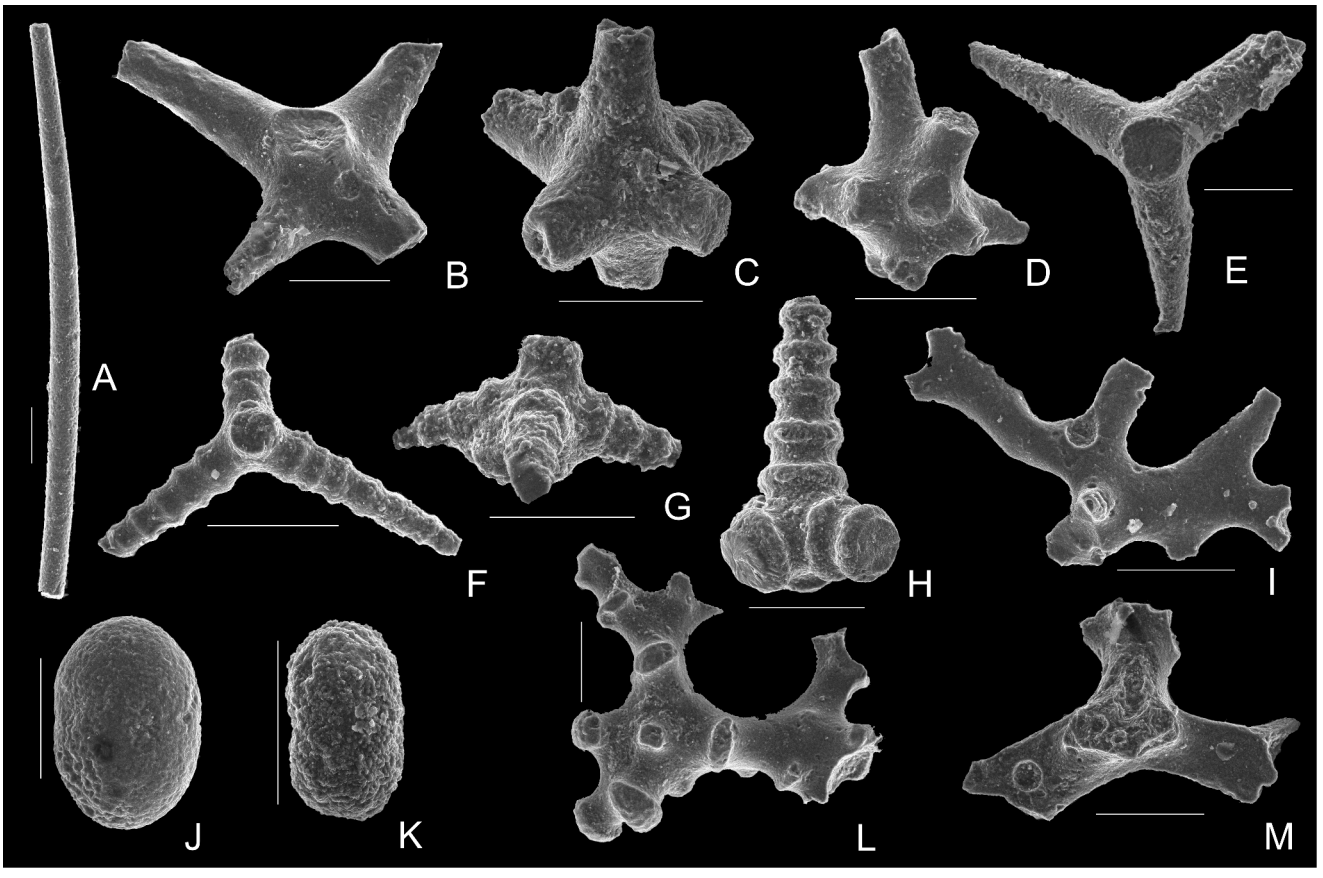

Fig. 6. Redeposited sponge spicules from shale parts of the Upper Cenomanian calciturbidites: **A** – Oxea (demosponge spicule; sample Krz-77); **B** – Partly broken massive dermal pentactine (hexactinellid spicule; Krz-76); **C** – Massive hexactine (hexactinellid spicule; Krz-76); **D** – Part of choanosomal skeleton (hexactinellid skeleton; Krz-82); **E** – Calthrop (demosponge spicule; Krz-78); **F**–**H** – Criccalthrop (demosponge spicule; F – Krz-81; G – Krz-75; H – Krz-76); **I** – Dermal phyllotriaene (demosponge spicule; Krz-76); **J, K** – Selenaster (demosponge spicule; J – Krz-77; K – Krz-75); **L** – ?Dicranoclone (demosponge desma; Krz-77); **M** – Demosponge spicule (Krz-66). Length of scale bar – 100 μm

The second level of the Fe-Mn layer with macronodules, underlain directly by a thin layer of green and black, organic-rich shale, occurs in the uppermost part of this succession (Fig. 3). Both layers lie in the same stratigraphic position as similar sediments in the CTB sections from the Silesian and Subsilesian nappes (Outer Carpathians). The chemical and mineralogical compositions, and the internal structures of the Fe-Mn layer is similar to the corresponding sediment from the Silesian Nappe (Bąk K., 2006, 2007a, b).

Variegated non-calcareous shales

The Variegated Shales are dominated by green non-calcareous shales with intercalations of red shale layers, 0.5–2 cm thick, and very thin laminae (< 0.5 mm) of silt-sized quartz, micas and sponge spicules. These sediments are tectonically sheared, occurring in two packages, 4.0 m and 1.2 m thick, respectively (Fig. 3). The lower package includes two thin layers of black, organic-rich shale with high TOC values (up to nearly 18%; Bąk K., 2007b), separated by a layer of grey clayey shale (?bentonite). Some green and red shale layers are enriched in Fe-Mn oxy-hydroxides, present as encrustations or filling-cracks (Fig. 9).

Microfossils (radiolarians and foraminifers) are more common in this series than in the underlying sediments. The radiolarian assemblages here are more diversified. They include stratigraphically important species such as *Patellula andrusovi* (Bąk M. *et al.*, 2005), which appears in Carpathian sequences above the organic-rich sediments (Bąk M., 2004). The first package of variegated shales, directly overlying the BRSF (9.7–13.7 from the base of the section), is devoid of any foraminifers and trace fossils. Poorly- to moderately-diversified DWAF assemblages occur in the second package of variegated shales, which is in tectonic contact with the underlying sediments. These assemblages consist of forms typical of sediments underlying the organic-rich series, like *Recurvoides* sp. (Fig. 10A, B), ?*Thalmannammina* sp. (Fig. 10C), *Trochammina* sp. (Fig. 10D, E), *Glomospira glomerata* (Fig. 10G), and additionally they include numerous infaunal forms belonging to *Gerochammina* spp. (Fig. 10F), *Bulbobaculites problematicus*, *Ammobaculites* sp. (Fig. 10H), *Uvigerinammina praejankoi* Neagu (Fig. 10I), and *U. jankoi* Majzon (Fig. 10J).

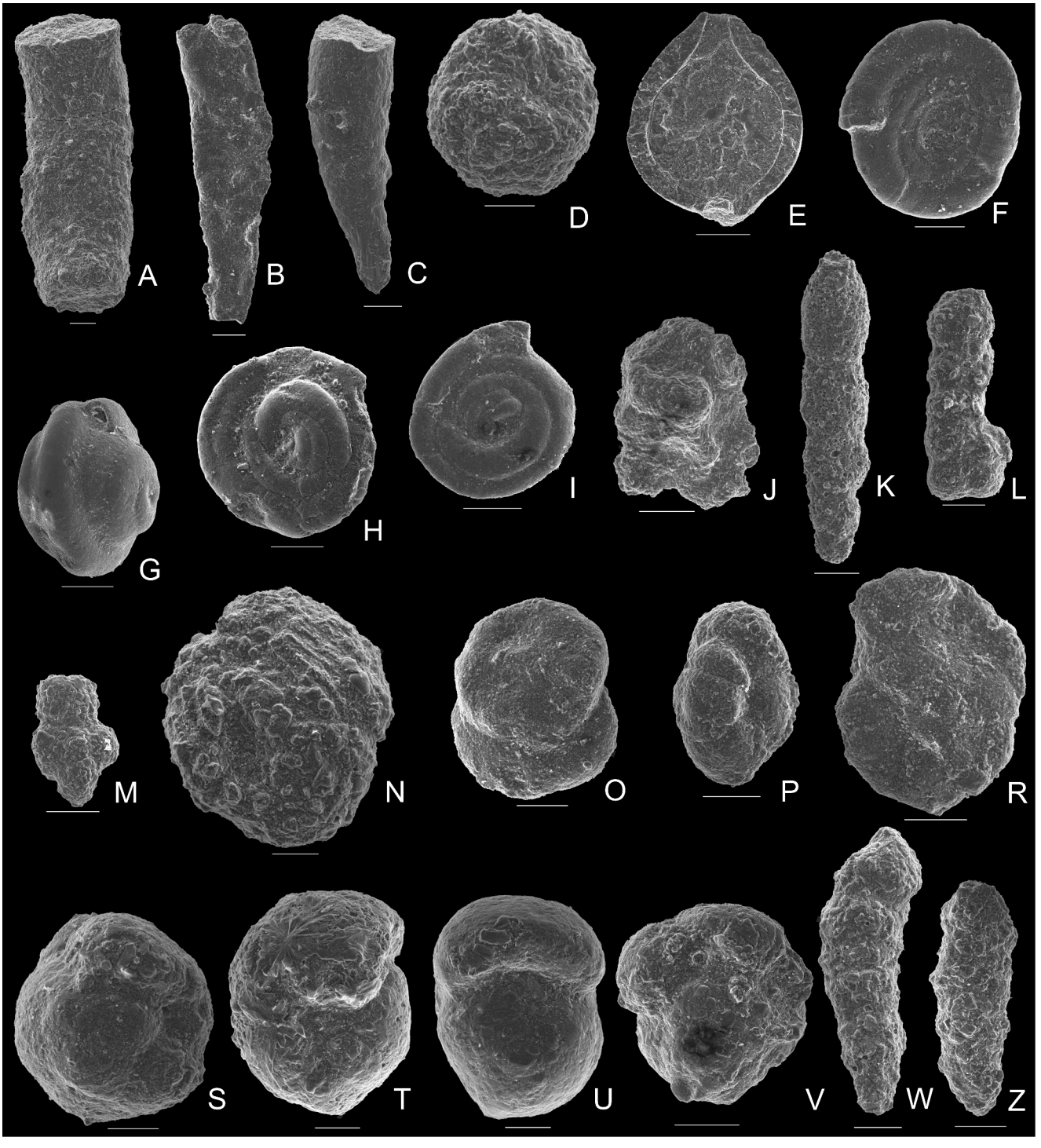

Fig. 7. SEM micrographs of the most common deep-water agglutinated foraminifers from the Upper Cenomanian hemipelagic shales: **A** – *Rhabdammina* sp. (sample Krz-89); **B** – *Hyperammina* sp. (Krz-89); **C** – *Hippocrepina depressa* Vašiček (Krz-87); **D** – *Psammosphaera* sp. (Krz-90); **E** – *Caudammina ovula* (Grzybowski) (Krz-87); **F** – *Ammodiscus cretaceus* (Reuss) (Krz-78); **G** – *Glomospira charoides* (Jones & Parker) (Krz-82); **H** – *Glomospira gordialis* (Jones & Parker) (Krz-94); **I** – *Glomospirella gaultina* (Berthelin) (Krz-94); **J** – *Glomospira irregularis* (Grzybowski) (Krz-76); **K** – *Pseudonodosinella parvula* (Huss) (Krz-89); **L** – *Bulbobaculites problematicus* (Neagu) (Krz-89); **M** – *Trochammina* sp. A (Krz-94); **N** – *Trochammina* sp. B (Krz-78); **O** – *Trochammina* sp. C (Krz-76); **P** – *Haplophragmoides* sp. A (Krz-78); **R** – *Haplophragmoides* cf. *walteri* (Grzybowski) (Krz-89); **S** – *Thalmannamina meandertornata* Neagu & Tocorjescu (Krz-87); **T** – *Plectorecurvoides alternans* Noth (Krz-76); **U** – *Recurvoides imperfectus* (Hanzlíková) (Krz-87); **V** – *Thalmannammina subturbinata* (Grzybowski) (Krz-76); **W** – *Gerochammina stanislawi* Neagu (Krz-82); **Z** – *Gerochammina lenis* (Grzybowski) (Krz-82). Length of scale bar – 100 μm

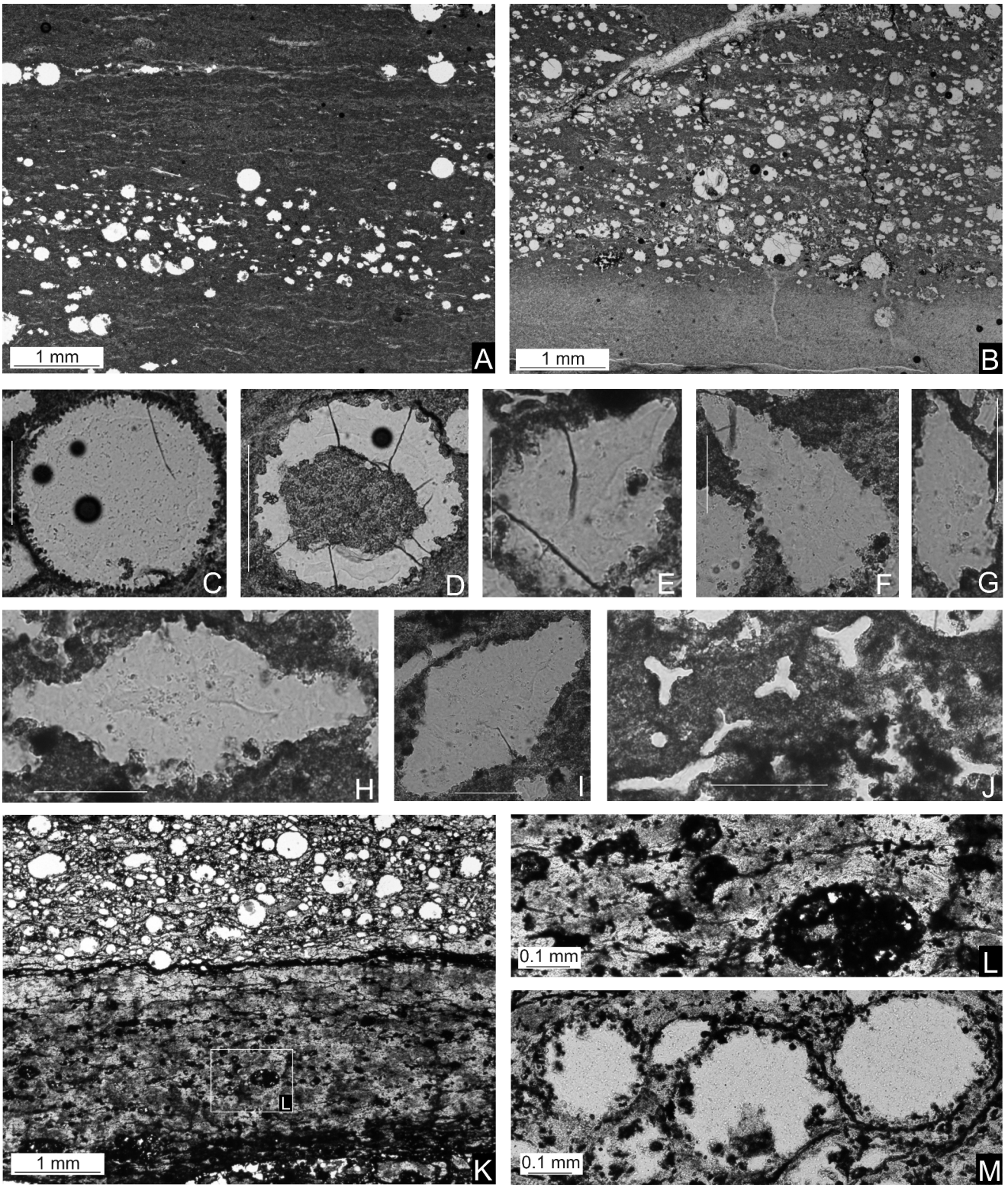

Fig. 8. **A, B** – Radiolarian-rich laminae within the lowermost Turonian green, siliceous-manganiferous shales (Krz-106d). **C–J** – Most frequent morphotypes of radiolarians (Krz-106d). **K–M** – Two radiolarian-rich laminae, consisting of skeletons entirely (L) and partly (M) filled with Fe-Mn oxide-hydroxides (Krz-106b); both laminae are separated by a thin Fe-Mn crust (M – radiolarian moulds from the upper laminae). Length of scale bar for C–J – 100 μm

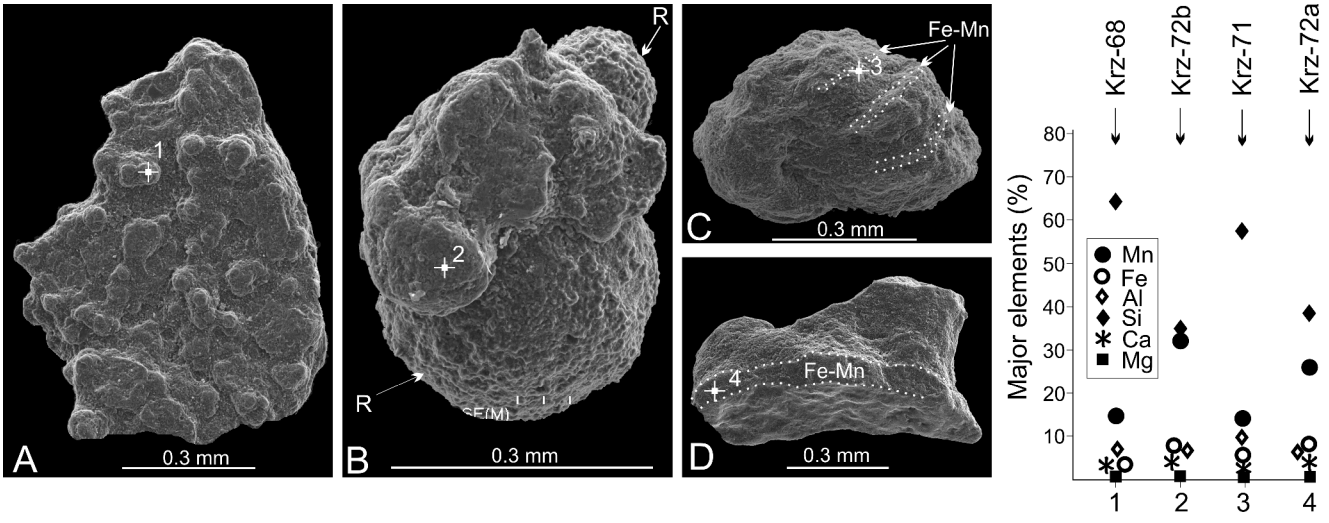

Fig. 9. **A**–**D** – Ferromanganese encrustations in Early Turonian variegated shales with contents of main elements (EDS analyses); R – radiolarian mould; 1–4: microprobe point analyses

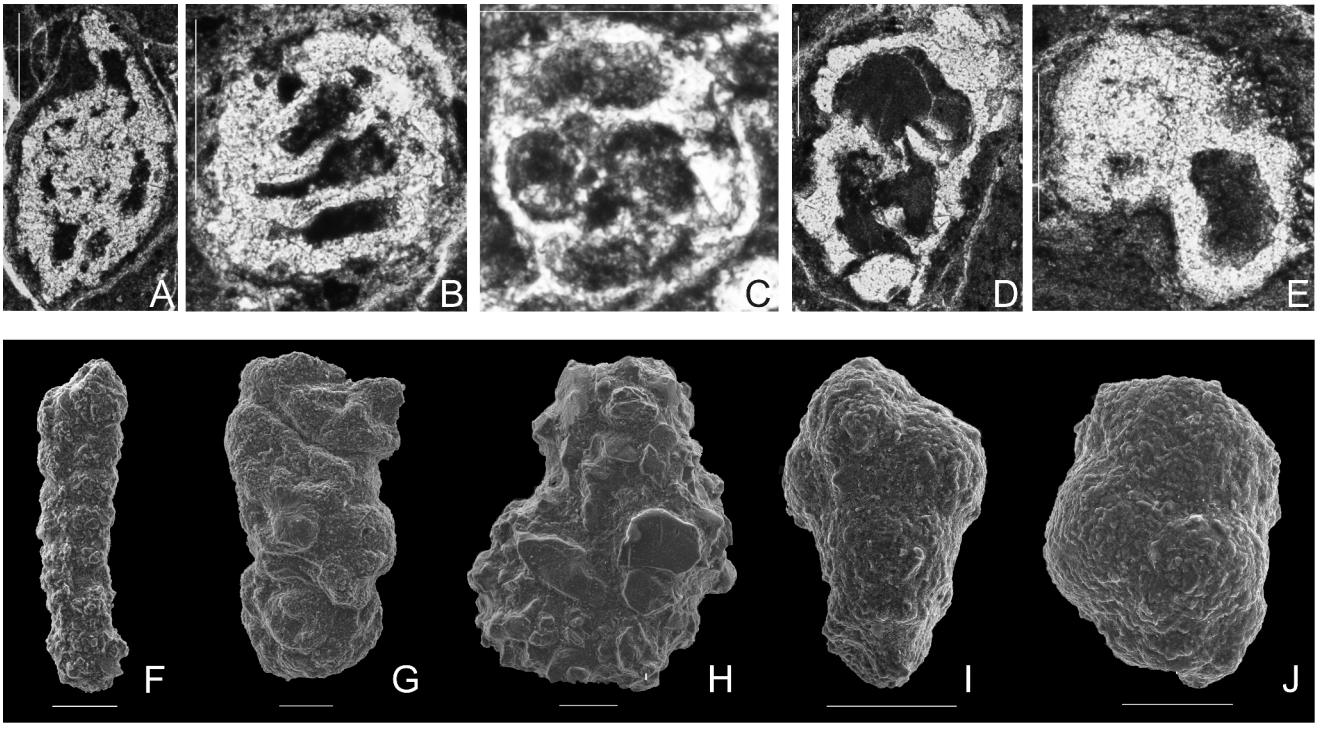

Fig. 10. Most frequent Early Turonian deep-water agglutinated foraminifers from variegated non-calcareous shales: **A, B** – *Recurvoides* sp.; **C** – ?*Thalmannammina* sp.; **D, E** – *Trochammina* sp. (A–E – thin section of sample Krz-61); **F** – *Gerochammina lenis* (Grzybowski) (Krz-60); **G** – *Glomospira glomerata* (Grzybowski) (Krz-61); **H** –*Ammobaculites* sp. (Krz-61); **I** – *Uvigerinammina praejankoi* Neagu (Krz-60); **J** – *Uvigerinammina jankoi* Majzon (Krz-60). Length of scale bar – 100 μm

Bulk sediment geochemistry

Geochemical indicators from the Spława section were used to interpret changes around the Cenomanian–Turonian boundary in detrital flux variations, oxygen content in bottom waters, and primary productivity. Thirteen samples from the marly shales, fifteen from the organic-rich series, one from the first Fe-Mn layer, and sixteen from the non-calcareous variegated shales were analyzed.

Indicators of detrital flux variations

Plots of Al_2O_3 vs. TiO_2 and Al_2O_3 vs. SiO_2 together with the Rb/Al, Ti/Al and Al/(Al+Fe+Mn) ratios have been made to determine detrital input to the seafloor.

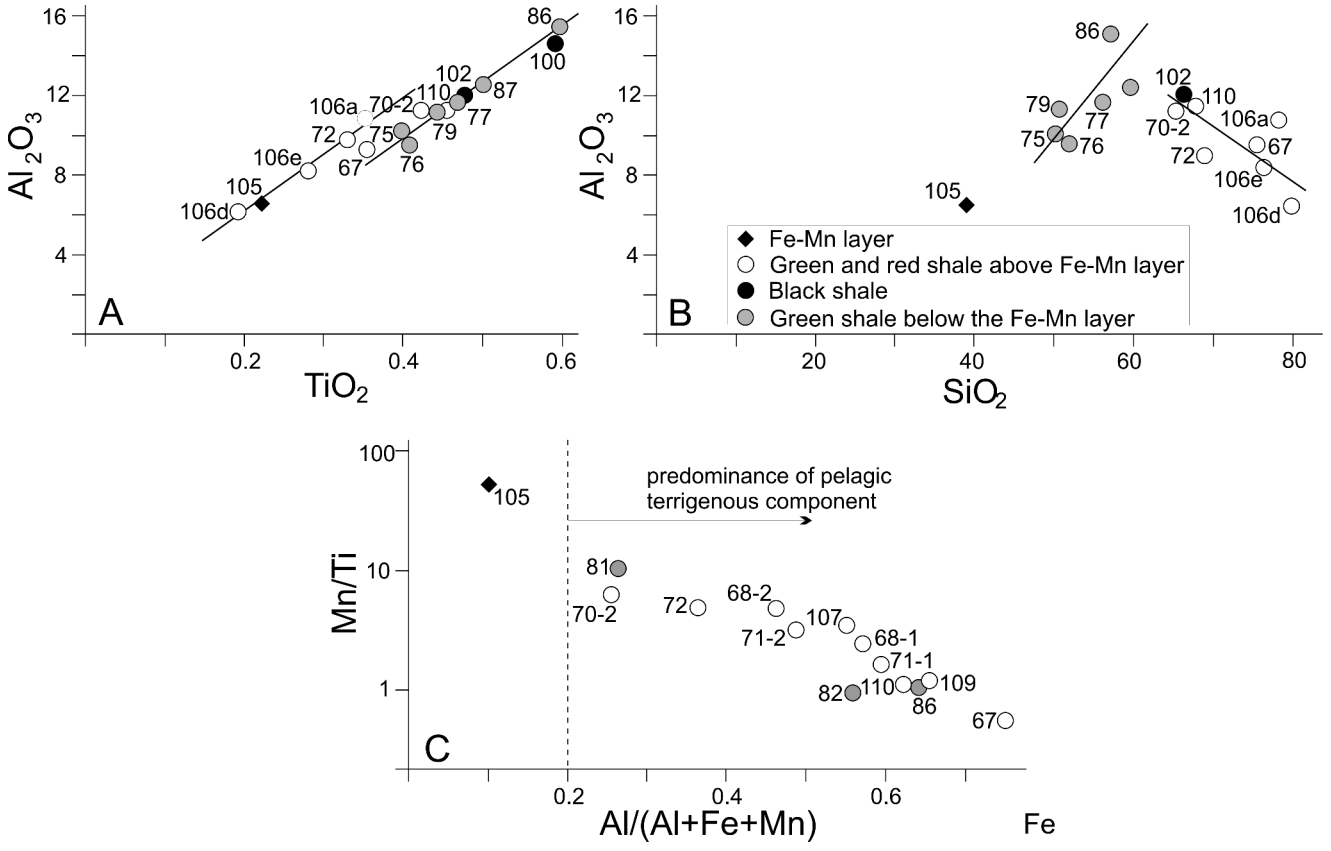

Fig. 11. Variation diagrams based on whole-rock data (**A–C**). In the SiO_2 vs. Al_2O_3 (**B**), the samples plot along two correlation lines. In the Al/(Al+Fe+Mn) vs. Mn/Ti plot (**C**), samples with Mn content exceeding 0.1% were plotted

Al_2O_3 and TiO_2 correlate well in most samples (Fig. 11A), which suggests their terrigenous origin. However, two different correlation lines are evident for the samples from the marl and organic-rich series, and for the Fe-Mn layer and overlying sediments. The latter sediments display the lowest contents of both Al_2O_3 and TiO_2.

Two distinct correlation lines can be also observed in a scatterplot of Al_2O_3 and SiO_2 (Fig. 11B). The first one can be related to the terrigenous origin of components in the Upper Cenomanian sediments below the first horizon of the Fe-Mn layer. The second one, expressed by a negative trend, characterizes the sediments above the Fe-Mn layer. This correlation may be explained by the biogenic origin of SiO_2 diluted by terrigenous particles. Biogenic silica originated from radiolarians as is shown by studies of the microfacies.

Another indicator of detrital input to the basin floor is the Al/(Al+Fe+Mn) ratio (Machhlour *et al.*, 1994). Its value decreases up section (Fig. 12), from a mean value of 0.63 in the marly shales, through 0.59 in the organic-rich series, to 0.52 in the variegated shales, suggesting a decrease in terrigenous supply to the sediment. It reaches the absolute minimum (0.11) in the first horizon of the Fe-Mn layer. In the organic-rich series, green shales display higher values of this ratio than those in the intercalated black shales, indicating a periodically enhanced rate of terrigenous supply during deposition time.

A decreasing trend is evident in the Ti/Al profile, regarded as a proxy for aeolian input (e.g., Wehausen & Brumsack, 1998). This trend, expressed by mean values, is present from the base of the section through the organic-rich succession (Fig. 12), but higher up the Ti/Al values rise again in the package of siliceous-manganiferous shales, which overlie the Fe-Mn layer, and decrease in the overlying variegated shales. The highest values of Ti/Al in the siliceous-manganiferous shales are not linked with the increase of Ti, as the values are even lower than in the neighbouring sediments, but they are related to significantly lower values of Al.

There are no distinct changes in the mean values of the Rb/Al ratio (Fig. 12), which is interpreted as an indicator of fluvial, fine detritus input (e.g., Wehausen & Brumsack, 1998), except for the green shales directly overlying the Fe-Mn layer. The maximum in the latter sediment is of the same origin as that mentioned above in the Ti/Al ratio.

The Rb/Al and Ti/Al ratios in the green shales from the organic-rich facies display higher values than in the intercalated black shales, that is suggestive of times of strengthened terrigenous supply to the basin floor, similarly as for the Al/(Al+Fe+Mn) ratio discussed above.

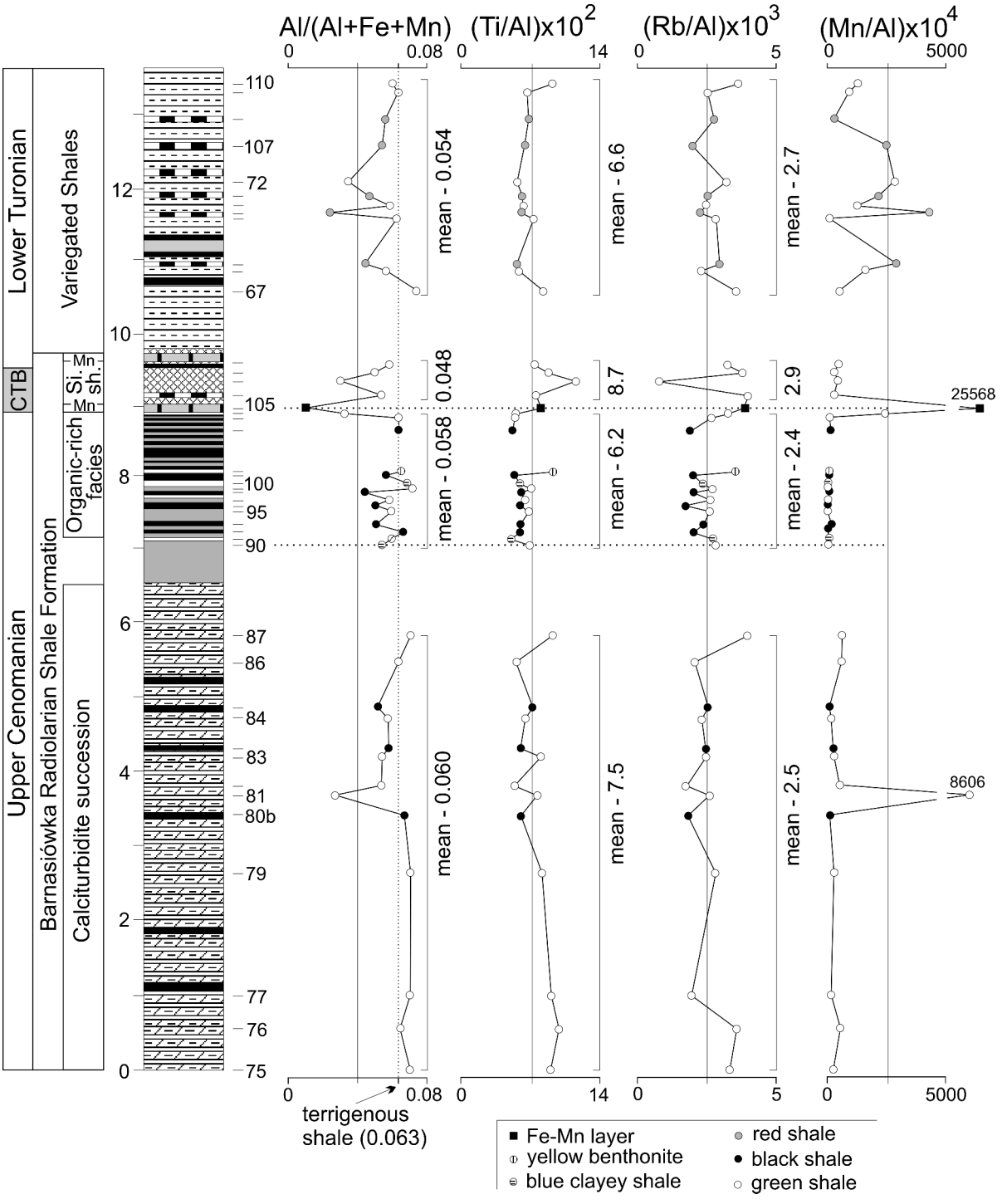

Fig. 12. Distribution of values of Al/(Al+Fe+Mn), Ti/Al and Rb/Al in the Spława section. For explanations of stratigraphical log – see Fig. 3. Dashed lines correspond to the organic-rich Bonarelli-equivalent series

Indicators of redox conditions

Redox conditions are evaluated from the U/Th, V/(V+Ni), and As/Al ratios. Their positive excursions are indicative of decreasing amounts of oxygen in bottom waters (e.g., Jones & Manning, 1994; McManus *et al.*, 1998; Hatch & Leventhal, 1992; Minami & Kato, 1997).

The U/Th ratio shows an elevated profile within the organic-rich facies (Fig. 13) and small fluctuations within the underlying shales of the calciturbidite succession, with maxima in the black shales. This suggests relatively lower oxygen levels during the deposition of the black shales, both within the middle and lower segments of the section.

Most values of the V/(V+Ni) ratio in the organic-rich facies and underlying hemipelagic shales within the marl series fall between 0.54 and 0.80 (Fig. 13), the range that was proposed as indicative of anoxic conditions (Hatch &

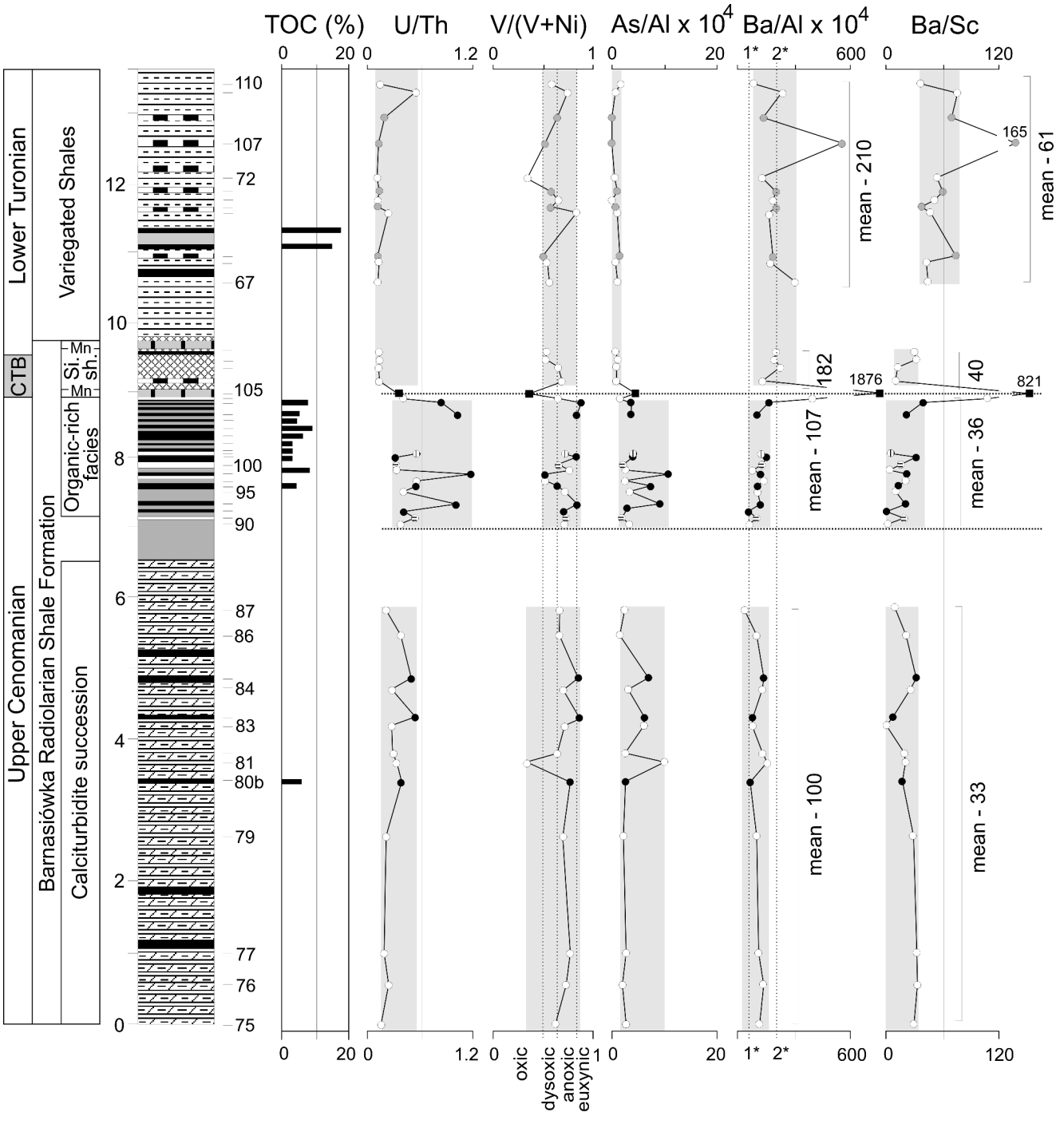

Fig. 13. Distribution of values of total organic carbon (TOC; after Bąk K., 2007b), U/Th, V/(V+Ni), (As/Al)x10^4, (Ba/Al)x10^4 and Ba/Sc in the Spława section. For explanations of stratigraphical log – see Fig. 3. Horizontal dashed lines correspond to the organic-rich facies (Bonarelli-equivalent horizon). 1* – Average shale (Wedepohl, 1971, 1991); 2* – CTBE black shales (Arthur *et al.*, 1990; Warning & Brumsack, 2000)

Leventhal, 1992). Some values exceed 0.80, suggesting even euxinic conditions. In contrast, most of the green and variegated shales overlying the first Fe-Mn layer show values close to 0.54 or lower, suggestive of dysoxic to oxic conditions at the seafloor.

Profiles of As/Al correlate well with those of U/Th and V/(V+Ni) (Fig. 13). Arsenic concentrations are elevated in the black shales, both in the lower and middle parts of the section. On the other hand, extremely low values are typical of the sediments overlying the first Fe-Mn layer. The simi-

larity of the As/Al, U/Th and V/(V+Ni) plot patterns are related to similar levels of concentration of organic matter. Under suboxic conditions, arsenic might occur as As_2S_3 and As_2S_5, associated with Fe sulfides (Farmer & Lovell, 1986; Minami & Kato, 1997). An enhanced content of As in the Fe-Mn layer is related to its diagenetic recycling. The As enrichment is probably associated with Fe in the form of arsenate absorbed on Fe oxides and hydroxides or as precipitated $FeAsO_4$ (e.g., Ferguson & Gavis, 1972). A high content of As/Al in the marly shale layer (Krz-81) in the lower part of the section is an effect of extremely low content of Al rather than the high content of As.

Indicators of productivity

Changes in the Ba/Al and Ba/Sc ratios are here used to interpret palaeoproductivity variations. Nevertheless, it should be stressed that solid-phase barium records could be unreliable as quantitative indicators for the history of ocean productivity in environments that have undergone suboxic diagenesis (Dehairs *et al.*, 1980; Dymond *et al.*, 1992; Schroeder *et al.*, 1997; Wehausen & Brumsack, 1998). Consequently, this analysis should be made only in conjunction with an analysis of redox conditions at the sea floor (McManus *et al.*, 1998).

A study of the Ba content shows that its fluxes are dominated by biogenic sources, but other sources, such as detrital aluminosilicates and hydrothermal precipitates may also contribute to the Ba preserved in deep-sea sediments (e.g., Dymond *et al.*, 1992). Additional problems in applying Ba as a palaeoproductivity proxy are due to processes controlling Ba preservation (Van Os *et al.*, 1991; McManus *et al.*, 1998). Its content might be reduced in low-oxygen conditions in bottom waters; a high rate of sulphate reduction also influences the preservation of Ba (Schenau *et al.*, 2001).

Although it is impossible to accurately estimate here the contribution of aluminosilicate particles to the Ba content, a normative analysis of the bulk sediment chemical compositions (Ba/Al ratio) may roughly delineate their significance. An additional indicator of palaeoproductivity could be the Ba/Sc ratio, as shown by Dickens and Owen (1996) on the basis of an assumption that Sc is predominantly hosted in aluminosilicates and Ba comes from abundant barite particles.

The negative correlation between the redox chemical indicators and the Ba/Al ratios for the organic-rich facies and black sediments in the underlying marl series precludes interpretation of productivity values for these sediments. Consequently, the only comparison could be made for the green marly shales of the calciturbidite series and the non-calcareous variegated shales above the first Fe-Mn layer. The data plot in Fig. 13 show a distinct increase in Ba/Al and Ba/Sc ratios in the variegated shales. Surprisingly, high Ba/Al and Ba/Sc ratios, associated with barium manganese oxides, occur in the first Fe-Mn layer above the organic-rich sediments. High values of Ba/Al and Ba/Sc ratios characterize also one of the red shale layers within the variegated shales (sample Krz-107; Fig. 13). They coincide with low values of terrigenous supply indices, suggesting a low clastic supply to the seafloor, indicative of enhanced biogenic Ba flux.

Manganese enrichments

Besides the two horizons of the Fe-Mn layer, enrichments in Mn oxide-hydroxides were also found in the underlying calcareous shale in the calciturbidite succession (up to 0.55%), and in the overlying non-calcareous variegated shales (up to 1.5%; Fig. 12). The Fe-Mn oxide-hydroxide enrichments occur mainly as diagenetic infillings of cracks and micro-encrustations.

To express the proportion of terrigenous versus hydrothermal contributions to these Fe-Mn sediments, the Mn/Ti *vs*. Al/(Al+Fe+Mn) diagram has been used (Rantisch *et al.*, 2003). The ratio of Al/(Al+Fe+Mn) is an indicator for clastic contribution to metalliferous sediments. The presented data (Tab. 1) plot on the domain indicating the predominance of a terrigenous component (Fig. 11), characterized by a chemical composition similar to average continental crust (Rantisch *et al.*, 2003).

DISCUSSION

Late Cenomanian calciturbidite sedimentation

The source of biogenic material in the calciturbidites was the shelf of the marginal part of the West European Platform. The transport direction (from north) is here proposed on the basis of facies analyses of the underlying sediments (Książkiewicz, 1962), because no flute casts were found in the turbidite beds in the studied series. The microfacies suggest low density gravity flows. The dominance of parallel lamination and extremely rare cross-lamination indicate their low velocities.

Neritic–upper bathyal depths are suggested for the environment from which the biogenic material was redeposited, on the basis of calcareous benthic foraminifers from the packstone and grainstone laminae. The benthic assemblages are dominated by small gavelinellids and the genus *Gyroidinoides*, accompaning *Lenticulina*, *Dentalina*, and *Nodosaria*. Such assemblages resemble those from outer distal ramp facies and their transition to upper slope facies, as described from the Cenomanian deposits of the Basque–Cantabrian Basin, at the northern continental margin of Iberia (Gräfe, 2005). Similar assemblages of the same age, with numerous gavelinellids are known from epicontinental seas in the southern part of the West European Platform, both from the carbonate (Polish Lowlands: Gawor-Biedowa, 1972; Heller, 1975; Peryt, 1983) and siltstone facies (Bohemian Cretaceous Basin: Hradecka, 1993; Hradecka & Švábenicka, 1995). They were also noted in marls from the NW-European continental shelves (e.g., Hart & Swiecicki, 1988). The neritic–upper bathyal depths could be confirmed by the relatively numerous occurrences of glauconite grains, which are thought to form mainly on the open shelf and upper slope environment (e.g., McRae, 1972; Amorosi, 1997).

Table 1

Major element and trace element chemistry for the Upper Cenomanian–Lower Turonian sediments recovered from the Spława section of the Skole Nappe, Outer Carpathians

	Sample no	Krz-75	Krz-76	Krz-77	Krz-79	Krz-80B	Krz-81	Krz-82	Krz-83-1	Krz-83A	Krz-84	Krz-84B	Krz-86
Ag	ppm	0.3	0.6	0.5	0.5	1.8	<d.l.	<d.l.	<d.l.	0.6	<d.l.	<d.l.	1.7
Al	%	2.71	2.55	3.1	3.22	4.53	0.64	2.83	3.25	3.85	3.98	4.07	3.33
As	ppm	6.7	4.8	7.9	6.5	11.4	12.6	6.9	19.5	23.4	11.2	28.4	4.6
Au	ppb	<d.l.	5	9	<d.l.	19	6	<d.l.	13	15	<d.l.	<d.l.	10
Ba	ppm	300	310	331	301	288	100	336	240	290	480	528	336
Be	ppm	1	1	2	2	2	<d.l.	1	<d.l.	<d.l.	2	2	1
Bi	ppm	<d.l.	<d.l.	<d.l.	<d.l.	<d.l.	<d.l.	<d.l.	<d.l.	<d.l.	<d.l.	<d.l.	<d.l.
Br	ppm	<d.l.	<d.l.	<d.l.	<d.l.	8.3	1.7	2.4	<d.l.	4	1.4	5	<d.l.
Ca	%	9.73	9.34	5.93	8.27	2.63	19.41	11.94	9.55	9.9	5.78	1.21	9.98
Cd	ppm	<d.l.	0.6	1	<d.l.	0.5	0.6	0.3	1.2	1.4	0.7	0.4	0.4
Co	ppm	14	12	17	16	28	8	11	13	23	13	14	13
Cr	ppm	59	68	84	79	153	23	51	71	150	69	154	60
Cs	ppm	5	5	4	5	6	1	4	6	4	8	9	6
Cu	ppm	85	65	73	102	258	67	64	71	146	131	231	83
Fe	%	2.23	2.34	2.56	2.57	2.21	1.25	2.11	2.59	2.62	2.77	3.4	3.09
Hf	ppm	2	3	4	3	2	5	2	4	<d.l.	3	2	2
K	%	1.53	1.57	1.76	1.76	2.07	0.29	1.17	1.69	1.49	1.91	2.16	2.41
Mg	%	0.86	0.82	0.98	0.95	1.3	0.24	0.79	0.92	0.93	1.17	1.21	1.24
Mn	ppm	640	1310	392	678	287	5508	1410	879	859	651	293	2021
Mo	ppm	<d.l.	<d.l.	<d.l.	<d.l.	2	<d.l.	<d.l.	<d.l.	<d.l.	<d.l.	<d.l.	<d.l.
Na	%	0.12	0.17	0.15	0.15	0.13	0.07	0.13	0.13	0.12	0.14	0.16	0.17
Ni	ppm	43	34	38	45	151	28	31	42	120	40	98	33
P	%	0.044	0.07	0.057	0.061	0.064	0.044	0.035	0.037	0.066	0.042	0.068	0.057
Pb	ppm	48	17	28	31	42	22	23	29	36	24	52	25
Rb	ppm	90	90	60	90	80	0	48	78	93	90	102	70
S	ppm	260	240	110	230	830	770	390	260	960	280	380	340
Sb	ppm	0.3	0.3	0.6	0.7	1	0.9	0.5	<d.l.	1.4	0.7	2	0.3
Sc	ppm	11	10	11	12	8	2.5	8.6	11.2	9.5	10.4	10.4	8.2
Se	ppm	<d.l.	<d.l.	<d.l.	<d.l.	<d.l.	<d.l.	<d.l.	<d.l.	<d.l.	<d.l.	<d.l.	<d.l.
Sn	ppm	<d.l.	<d.l.	<d.l.	<d.l.	<d.l.	<d.l.	<d.l.	<d.l.	<d.l.	<d.l.	<d.l.	<d.l.
Sr	ppm	248	145	158	189	125	283	376	269	259	219	100	324
Ta	ppm	<d.l.	<d.l.	<d.l.	<d.l.	<d.l.	0.6	<d.l.	<d.l.	<d.l.	<d.l.	<d.l.	<d.l.
Th	ppm	9.4	9.7	11.3	9.9	9.7	3.1	7.3	9.1	8	9	10.5	7.5
Ti	%	0.24	0.25	0.28	0.26	0.27	0.05	0.15	0.26	0.23	0.25	0.29	0.19
U	ppm	1.4	2.1	2	2.1	3.5	0.9	2	2.4	4.1	2.2	4.7	2.7
V	ppm	70	79	116	89	492	14	51	99	637	84	492	63
W	ppm	<d.l.	<d.l.	<d.l.	<d.l.	<d.l.	<d.l.	<d.l.	<d.l.	<d.l.	<d.l.	<d.l.	<d.l.
Y	ppm	22	24	23	25	21	25	17	17	31	17	19	19
Zn	ppm	69	58	111	76	179	21	37	104	183	93	223	74
Zr	ppm	72	87	104	80	n.d.	n.d.	n.d.	n.d.	n.d.	n.d.	n.d.	99
La	ppm	30.4	27.5	32.9	32.1	26.1	22.9	24.4	23.3	28.2	30.2	33.8	24.3
Ce	ppm	63	56	68	69	54	46	48	47	72	58	75	54
Nd	ppm	23	23	25	30	28	20	24	22	19	25	34	21
Sm	ppm	5.8	5.7	6	6.6	4.6	3.7	3.8	3.5	5.7	4.3	5.8	3.9
Eu	ppm	1.2	1.2	1.2	1.3	1.1	1	1	0.8	1.4	1.4	1.1	1.3
Tb	ppm	<d.l.	<d.l.	<d.l.	<d.l.	<d.l.	0.7	0.6	<d.l.	<d.l.	<d.l.	<d.l.	<d.l.
Yb	ppm	2.2	2.3	2.3	2.3	1.3	2.1	1.6	1.9	2.1	1.7	1.5	1.5
Lu	ppm	0.36	0.39	0.35	0.36	0.17	0.33	0.25	0.35	0.32	0.26	0.26	0.21
Ce/La		2.1	2	2.1	2.1	2.1	2	2	2	2.6	1.9	2.2	2.2

Table 1 continued

	Sample no	Krz-87	Krz-90	Krz-91	Krz-106c	Krz-106d	Krz-106e	Krz-107	Krz-108	Krz-109	Krz-110	Krz-67
Ag	ppm	0.5	<d.l.	<d.l.	<d.l.	<d.l.	<d.l.	<d.l.	<d.l.	<d.l.	0.3	0.3
Al	%	3.31	4.55	5.52	1.82	1.64	2.18	3.08	3.56	3.61	2.94	2.52
As	ppm	7.1	13.8	9.2	1.2	1.7	1.4	3	2.1	4.7	2.4	1.4
Au	ppb	2	10	<d.l.	<d.l.	<d.l.	<d.l.	<d.l.	<d.l.	5	<d.l.	<d.l.
Ba	ppm	117	304	528	400	310	429	1680	448	800	874	382
Be	ppm	2	2	3	2	0	<d.l.	2	2	2	2	1
Bi	ppm	<d.l.	<d.l.	<d.l.	<d.l.	<d.l.	<d.l.	<d.l.	<d.l.	<d.l.	<d.l.	<d.l.
Br	ppm	<d.l.	<d.l.	<d.l.	<d.l.	<d.l.	<d.l.	<d.l.	<d.l.	<d.l.	<d.l.	<d.l.
Ca	%	4.15	0.91	0.88	0.81	0.39	0.55	0.7	0.73	0.8	0.76	0.62
Cd	ppm	1	0.4	0.4	0.5	<d.l.	<d.l.	0.4	<d.l.	0.4	0.6	0.5
Co	ppm	24	20	6	11	6	7	18	15	17	22	9
Cr	ppm	79	74	94	80	30	51	65	94	82	80	64
Cs	ppm	7	9	10	3	3	3	6	8	8	5	5
Cu	ppm	84	325	75	132	105	83	99	50	120	184	43
Fe	%	5.27	3.7	3.57	4.18	3.31	2.86	1.75	2.53	1.61	2.88	5.21
Hf	ppm	3	2	3	2	<d.l.	2	2	3	2	3	2
K	%	2.44	2.36	2.6	1.5	1.17	1.35	1.42	1.92	1.74	2.01	1.55
Mg	%	1.03	1.39	1.54	0.8	0.53	0.71	1	1.15	1.15	1.04	0.76
Mn	ppm	1213	428	419	335	346	904	7414	847	3095	3782	1062
Mo	ppm	<d.l.	4	<d.l.	<d.l.	<d.l.	<d.l.	<d.l.	<d.l.	<d.l.	<d.l.	<d.l.
Na	%	0.17	0.18	0.17	0.21	0.13	0.17	0.19	0.2	0.18	0.16	0.13
Ni	ppm	53	50	46	49	37	47	64	53	44	66	55
P	%	0.061	0.067	0.05	0.101	0.052	0.7	0.043	0.042	0.068	0.039	0.026
Pb	ppm	19	45	27	7	13	6	16	16	33	15	7
Rb	ppm	130	128	148	<d.l.	60	70	62	101	89	110	90
S	ppm	80	5780	100	<d.l.	10	20	40	50	70	20	20
Sb	ppm	0.4	1.6	1	0.6	0.5	0.4	0.6	0.7	0.6	0.5	0.4
Sc	ppm	12	13.3	13.9	12	6	9	10.2	10.8	11.1	19	10
Se	ppm	<d.l.	<d.l.	<d.l.	<d.l.	<d.l.	<d.l.	<d.l.	<d.l.	<d.l.	<d.l.	<d.l.
Sn	ppm	<d.l.	<d.l.	<d.l.	<d.l.	<d.l.	<d.l.	<d.l.	<d.l.	<d.l.	<d.l.	<d.l.
Sr	ppm	140	92	96	69	47	62	84	79	80	72	47
Ta	ppm	<d.l.	<d.l.	1	<d.l.	<d.l.	<d.l.	<d.l.	<d.l.	<d.l.	<d.l.	<d.l.
Th	ppm	11.5	11.2	10.5	7.7	5.3	7.3	8.7	9.4	8.9	8.9	8.2
Ti	%	0.31	0.31	0.27	0.21	0.11	0.16	0.19	0.24	0.23	0.27	0.21
U	ppm	2.3	4	4.8	1	0.8	1	1.1	1.8	4.4	1.4	1
V	ppm	94	113	119	84	38	52	66	97	119	94	72
W	ppm	2	<d.l.	<d.l.	<d.l.	<d.l.	2	<d.l.	<d.l.	<d.l.	<d.l.	2
Y	ppm	26	20	21	29	17	23	21	18	34	19	15
Zn	ppm	109	100	93	61	49	57	79	91	100	94	84
Zr	ppm	94	n.d.	n.d.	n.d.	32	51	n.d.	n.d.	n.d.	82	56
La	ppm	31.6	34.4	36.2	41.2	16.1	22.7	29.9	27.8	38.6	26.5	19.4
Ce	ppm	60	82	85	104	41	56	74	60	92	61	46
Nd	ppm	25	22	33	33	14	21	34	23	31	20	15
Sm	ppm	5.8	5.4	4.7	7.7	2.9	4.5	5.1	3.8	7	4.8	3.5
Eu	ppm	1.2	1	2.1	1.6	0.6	0.9	1.3	1	1.8	1	0.6
Tb	ppm	<d.l.	<d.l.	<d.l.	<d.l.	<d.l.	<d.l.	<d.l.	<d.l.	1	<d.l.	<d.l.
Yb	ppm	2.3	2.2	2.2	3.9	1.7	2.2	0	0	1	2.4	1.8
Lu	ppm	0.4	0.37	0.38	0.52	0.28	0.33	0.33	0.41	0.44	0.37	0.3
Ce/La		1.9	2.4	2.3	2.5	2.5	2.5	2.5	2.2	2.4	2.3	2.4

Table 1 continued

	Sampe no	Krz-68-01	Krz-68-02	Krz-70-01	Krz-70-02	Krz-71-01	Krz-71-02	Krz-72	Krz-106c	Krz-106d	Krz-106e	Krz-107
Ag	ppm	<d.l.	<d.l.	<d.l.	<d.l.	<d.l.	<d.l.	<d.l.	<d.l.	<d.l.	<d.l.	<d.l.
Al	%	3.43	3.48	3.63	3.61	3.78	4.12	3.76	1.82	1.64	2.18	3.08
As	ppm	<d.l.	2.7	1.8	<d.l.	<d.l.	2.4	6.3	1.2	1.7	1.4	3
Au	ppb	<d.l.	<d.l.	<d.l.	<d.l.	<d.l.	<d.l.	<d.l.	<d.l.	<d.l.	<d.l.	<d.l.
Ba	ppm	464	648	592	728	696	800	440	400	310	429	1680
Be	ppm	2	2	2	2	2	2	<d.l.	2	0	<d.l.	2
Bi	ppm	<d.l.	<d.l.	3	<d.l.	<d.l.	<d.l.	5	<d.l.	<d.l.	<d.l.	<d.l.
Br	ppm	<d.l.	<d.l.	<d.l.	<d.l.	<d.l.	<d.l.	<d.l.	<d.l.	<d.l.	<d.l.	<d.l.
Ca	%	0.83	0.9	0.81	0.97	0.91	1.04	0.9	0.81	0.39	0.55	0.7
Cd	ppm	<d.l.	0.4	<d.l.	0.5	0.5	0.7	1	0.5	<d.l.	<d.l.	0.4
Co	ppm	14	25	14	28	16	22	14	11	6	7	18
Cr	ppm	53	64	82	72	58	58	65	80	30	51	65
Cs	ppm	6	8	8	10	6	8	5	3	3	3	6
Cu	ppm	338	631	41	61	55	39	102	132	105	83	99
Fe	%	2.09	3.87	2.03	3.88	2.13	3.68	5.7	4.18	3.31	2.86	1.75
Hf	ppm	2	2	4	2	3	2	2	2	<d.l.	2	2
K	%	1.63	1.84	1.87	1.99	1.91	2.23	1.91	1.5	1.17	1.35	1.42
Mg	%	1.04	1.14	1.11	1.15	1.14	1.31	0.97	0.8	0.53	0.71	1
Mn	ppm	5644	9858	286	15159	4544	8745	10649	335	346	904	7414
Mo	ppm	<d.l.	<d.l.	<d.l.	2	<d.l.	2	2	<d.l.	<d.l.	<d.l.	<d.l.
Na	%	0.15	0.15	0.19	0.15	0.18	0.14	0.18	0.21	0.13	0.17	0.19
Ni	ppm	51	65	40	69	47	71	155	49	37	47	64
P	%	0.048	0.046	0.065	0.04	0.059	0.059	0.099	0.101	0.052	0.7	0.043
Pb	ppm	9	11	13	18	16	18	29	7	13	6	16
Rb	ppm	79	100	100	81	91	101	120	<d.l.	60	70	62
S	ppm	70	50	70	60	80	70	50	<d.l.	10	20	40
Sb	ppm	0.3	0.6	0.6	0.7	0.2	0.8	0.7	0.6	0.5	0.4	0.6
Sc	ppm	9.2	10.9	11.2	10.9	10.3	10.8	12	12	6	9	10.2
Se	ppm	<d.l.	<d.l.	<d.l.	<d.l.	<d.l.	<d.l.	<d.l.	<d.l.	<d.l.	<d.l.	<d.l.
Sn	ppm	<d.l.	<d.l.	<d.l.	<d.l.	<d.l.	<d.l.	<d.l.	<d.l.	<d.l.	<d.l.	<d.l.
Sr	ppm	57	56	60	60	64	66	62	69	47	62	84
Ta	ppm	<d.l.	<d.l.	1.1	<d.l.	<d.l.	<d.l.	<d.l.	<d.l.	<d.l.	<d.l.	<d.l.
Th	ppm	7.7	8.2	9.2	9.6	9.2	8.4	7.6	7.7	5.3	7.3	8.7
Ti	%	0.2	0.19	0.26	0.22	0.24	0.25	0.21	0.21	0.11	0.16	0.19
U	ppm	1	1	2	1.1	1.1	1.2	0.8	1	0.8	1	1.1
V	ppm	59	60	190	87	85	89	76	84	38	52	66
W	ppm	<d.l.	6	<d.l.	<d.l.	<d.l.	<d.l.	<d.l.	<d.l.	<d.l.	2	<d.l.
Y	ppm	26	25	28	22	30	29	52	29	17	23	21
Zn	ppm	78	88	0	95	97	102	180	61	49	57	79
Zr	ppm	n.d.	n.d.	n.d.	n.d.	n.d.	n.d.	60	n.d.	32	51	n.d.
La	ppm	29.4	32.8	36.4	33.2	34.2	32.4	33.2	41.2	16.1	22.7	29.9
Ce	ppm	67	76	89	82	86	77	100	104	41	56	74
Nd	ppm	25	29	38	32	30	30	31	33	14	21	34
Sm	ppm	5	5.4	6.5	5.3	6.1	5.8	7.1	7.7	2.9	4.5	5.1
Eu	ppm	1.4	1.4	1.7	1.3	1.6	1.4	1.9	1.6	0.6	0.9	1.3
Tb	ppm	0.9	<d.l.	<d.l.	<d.l.	<d.l.	<d.l.	<d.l.	<d.l.	<d.l.	<d.l.	<d.l.
Yb	ppm	2	2.2	2.2	2.2	2.4	2.2	3.4	3.9	1.7	2.2	0
Lu	ppm	0.3	0.38	0.38	0.35	0.43	0.43	0.55	0.52	0.28	0.33	0.33
Ce/La		2.3	2.3	2.4	2.5	2.5	2.4	3	2.5	2.5	2.5	2.5

Table 1 continued

	Sample no	Krz-108	Krz-109	Krz-110	Krz-67	Krz-68-01	Krz-68-02	Krz-70-01	Krz-70-02	Krz-71-01	Krz-71-02	Krz-72
Ag	ppm	<d.l.	<d.l.	0.3	0.3	<d.l.	<d.l.	<d.l.	<d.l.	<d.l.	<d.l.	<d.l.
Al	%	3.56	3.61	2.94	2.52	3.43	3.48	3.63	3.61	3.78	4.12	3.76
As	ppm	2.1	4.7	2.4	1.4	<d.l.	2.7	1.8	<d.l.	<d.l.	2.4	6.3
Au	ppb	<d.l.	5	<d.l.	<d.l.	<d.l.	<d.l.	<d.l.	<d.l.	<d.l.	<d.l.	<d.l.
Ba	ppm	448	800	874	382	464	648	592	728	696	800	440
Be	ppm	2	2	2	1	2	2	2	2	2	2	<d.l.
Bi	ppm	<d.l.	<d.l.	<d.l.	<d.l.	<d.l.	<d.l.	3	<d.l.	<d.l.	<d.l.	5
Br	ppm	<d.l.	<d.l.	<d.l.	<d.l.	<d.l.	<d.l.	<d.l.	<d.l.	<d.l.	<d.l.	<d.l.
Ca	%	0.73	0.8	0.76	0.62	0.83	0.9	0.81	0.97	0.91	1.04	0.9
Cd	ppm	<d.l.	0.4	0.6	0.5	<d.l.	0.4	<d.l.	0.5	0.5	0.7	1
Co	ppm	15	17	22	9	14	25	14	28	16	22	14
Cr	ppm	94	82	80	64	53	64	82	72	58	58	65
Cs	ppm	8	8	5	5	6	8	8	10	6	8	5
Cu	ppm	50	120	184	43	338	631	41	61	55	39	102
Fe	%	2.53	1.61	2.88	5.21	2.09	3.87	2.03	3.88	2.13	3.68	5.7
Hf	ppm	3	2	3	2	2	2	4	2	3	2	2
K	%	1.92	1.74	2.01	1.55	1.63	1.84	1.87	1.99	1.91	2.23	1.91
Mg	%	1.15	1.15	1.04	0.76	1.04	1.14	1.11	1.15	1.14	1.31	0.97
Mn	ppm	847	3095	3782	1062	5644	9858	286	15159	4544	8745	10649
Mo	ppm	<d.l.	<d.l.	<d.l.	<d.l.	<d.l.	<d.l.	<d.l.	2	<d.l.	2	2
Na	%	0.2	0.18	0.16	0.13	0.15	0.15	0.19	0.15	0.18	0.14	0.18
Ni	ppm	53	44	66	55	51	65	40	69	47	71	155
P	%	0.042	0.068	0.039	0.026	0.048	0.046	0.065	0.04	0.059	0.059	0.099
Pb	ppm	16	33	15	7	9	11	13	18	16	18	29
Rb	ppm	101	89	110	90	79	100	100	81	91	101	120
S	ppm	50	70	20	20	70	50	70	60	80	70	50
Sb	ppm	0.7	0.6	0.5	0.4	0.3	0.6	0.6	0.7	0.2	0.8	0.7
Sc	ppm	10.8	11.1	19	10	9.2	10.9	11.2	10.9	10.3	10.8	12
Se	ppm	<d.l.	<d.l.	<d.l.	<d.l.	<d.l.	<d.l.	<d.l.	<d.l.	<d.l.	<d.l.	<d.l.
Sn	ppm	<d.l.	<d.l.	<d.l.	<d.l.	<d.l.	<d.l.	<d.l.	<d.l.	<d.l.	<d.l.	<d.l.
Sr	ppm	79	80	72	47	57	56	60	60	64	66	62
Ta	ppm	<d.l.	<d.l.	<d.l.	<d.l.	<d.l.	<d.l.	1.1	<d.l.	<d.l.	<d.l.	<d.l.
Th	ppm	9.4	8.9	8.9	8.2	7.7	8.2	9.2	9.6	9.2	8.4	7.6
Ti	%	0.24	0.23	0.27	0.21	0.2	0.19	0.26	0.22	0.24	0.25	0.21
U	ppm	1.8	4.4	1.4	1	1	1	2	1.1	1.1	1.2	0.8
V	ppm	97	119	94	72	59	60	190	87	85	89	76
W	ppm	<d.l.	<d.l.	<d.l.	2	<d.l.	6	<d.l.	<d.l.	<d.l.	<d.l.	<d.l.
Y	ppm	18	34	19	15	26	25	28	22	30	29	52
Zn	ppm	91	100	94	84	78	88	0	95	97	102	180
Zr	ppm	n.d.	n.d.	82	56	n.d.	n.d.	n.d.	n.d.	n.d.	n.d.	60
La	ppm	27.8	38.6	26.5	19.4	29.4	32.8	36.4	33.2	34.2	32.4	33.2
Ce	ppm	60	92	61	46	67	76	89	82	86	77	100
Nd	ppm	23	31	20	15	25	29	38	32	30	30	31
Sm	ppm	3.8	7	4.8	3.5	5	5.4	6.5	5.3	6.1	5.8	7.1
Eu	ppm	1	1.8	1	0.6	1.4	1.4	1.7	1.3	1.6	1.4	1.9
Tb	ppm	<d.l.	1	<d.l.	<d.l.	0.9	<d.l.	<d.l.	<d.l.	<d.l.	<d.l.	<d.l.
Yb	ppm	0	1	2.4	1.8	2	2.2	2.2	2.2	2.4	2.2	3.4
Lu	ppm	0.41	0.44	0.37	0.3	0.3	0.38	0.38	0.35	0.43	0.43	0.55
Ce/La		2.2	2.4	2.3	2.4	2.3	2.3	2.4	2.5	2.5	2.4	3

Oxygenation of bottom-water fluctuated during the deposition of the calciturbidite succession. Frequent periods with dysoxic conditions are marked by numerous dark-grey layers, low-diversity of DWAF assemblages, *Chondrites* traces in the green layers, and the high values of chemical redox indexes of dark-grey sediments. A few black non-calcareous shale intercalations indicate anoxic or even euxinic conditions at the basin floor, on the basis of chemical indexes (Fig. 13) and the lack of benthic foraminifers.

The calciturbidite succession occurring in the studied section below the organic-rich facies is not unique in the Upper Cenomanian of the Outer Carpathians. Similar sediments, distinguished as the Mikuszowice Cherts (Burtanówna, 1933) lie in the same stratigraphic position (the Middle-Late Cenomanian: Bąk M. *et al.*, 2005) in the west, in other marginal basin of the Outer Carpathians, the Silesian Basin. These are spicule-rich turbidites including admixture of numerous radiolarian and calcareous benthic and planktonic foraminiferal particles. This biogenic material together with siliciclastic grains was supplied also from the margin of the West European Platform.

In both basins located along the northern margin of the Northern Tethys, turbidites with dominant biogenic material were replaced by organic-rich sediments during the same time, *i.e.* during the latest Cenomanian (Bąk K. *et al.*, 2001; Bąk M. *et al.*, 2005). It seems that their gradual disappearance was related to rising sea-level and to expansion of the oxygen minimum zone. The first factor, the ongoing eustatic sea-level rise (e.g., Jacquin & de Graciansky, 1998), limited the amount of continental silty and sandy detritus by flooding of continental shelves, while the second one, significantly restricted the development of macro- and microfauna at both the sea bottom and the surface.

Latest Cenomanian organic-rich sedimentation

The stratigraphic position of the organic-rich facies of the studied section (lower and middle parts of the carbon isotope excursion) shows that these sediments are the equivalent of the "Bonarelli level", recorded from deep-water carbonate facies in the Western Tethys (e.g., Arthur & Premoli Silva, 1982; Luciani & Cobianchi, 1999; Scopelliti *et al.*, 2004). The benthos-free, black shales, with TOC contents between 3 and 8% (Bąk K., 2007b), indicate anoxic or even euxinic conditions at the sea floor. Bottom-water anoxia is confirmed by positive excursions of chemical redox indices such as the U/Th, V/(V+Ni), and As/Al ratios, which have their maxima in the black shales (Fig. 13). Organic matter originated both from, terrestrial and marine sources (Bąk K., 2007b). One of the sources of the latter type of organic matter could be algae, what is inferred on the basis of the high values of the As/Al ratio in the black shale layer containing mainly marine organic matter (s. Krz-98; Fig. 13). Arsenic as a biophile element, absorbed by planktonic organisms (mainly by algae) in surface water (Francesconi & Edmonds, 1998) is scavenged from seawater to sediment by organic carbon matter fraction, in a manner similar to the behavior of Se, Sb, Ag, Zn and Br (Masuzawa, 1989). Besides algae, the marine organic matter enrichment is linked to the abundance of radiolarians; this may reflect enhanced productivity during the upwelling-controlled intervals.

Periods of bottom anoxia were interrupted by intervals with turbidite sedimentation. An increase in fine detrital input to the basin floor is marked by positive excursions of Al/(Al+Fe+Mn) and Rb/Al profiles. The latter are representative of dominant fluvial input, what may suggest that riverine discharge was a major source of fine detritus during the deposition of the green shales. The aeolian contribution in detrital input was negligible, as expressed by the Ti/Al ratio which is the lowest in comparison to the underlying and overlying sediments, probably reflecting the maximum of the worldwide transgression. The sedimentation of green shales occurred under dysoxic conditions, as testified by the chemical redox indices. Poorly-diversified DWAF assemblages in the green shales (Fig. 3), represented by the "Biofacies B" of Kuhnt and Kaminski (1989) confirm the oxygen-depleted conditions at the basin floor.

Reoxygenation of bottom water close to the C-T boundary

The precipitation of two horizons of the Fe-Mn layer overlying the organic-rich facies was related to changes in bottom water dynamics across the C–T boundary, as suggested by their mineralogical, chemical, and microfacies studies (Bąk K., 2007b). Both layers originated as rhodochrosite-rich sediment, formed under anoxic pore and/or bottom water that could be episodically oxydized by recurrent inflows of warm, oxygenated water transported by bottom currents (for details – see Bąk K., 2006). Most probably, during an increase in deep-water circulation, which caused the long-termed intervals with well-oxygenated bottom and pore-water in the topmost part of the sediments, the rhodochrosite-rich layer, including also numerous barite crystals, was diagenetically transformed into barium-manganese oxides. The palaeontological data, such as the numerous occurrence of a small-sized infaunal DWAF assemblage in the variegated shale directly overlying the Fe-Mn layer, which is simultaneously the first appearance of benthic foraminifers above the organic-rich facies, may support such a suggestion (Bąk K., 2007b).

The siliceous-manganiferous shale series between the two horizons of the Fe-Mn layer includes a few levels of very thin Fe-Mn crusts, which may correspond to periods of extremely low sedimentation rate or even hiatuses. Chemical indicators of detrital input to the basin floor, such as the Al/(Al+Fe+Mn) ratio (Machhlour *et al.*, 1994) have the lowest mean value in this series, demonstrating the lowest terrigenous supply to the basin floor within the whole studied section. The lowest content of Al_2O_3 in these sediments (Fig. 11A) supports this interpretation. All these features demonstrate that the siliceous-manganiferous shale series could correspond to period of high stand of sea level during the worldwide transgression, which prevented siliciclastic supply to the basin floor.

The oxygenation of the bottom- and pore-waters during Early Turonian times is also confirmed by the chemical redox indicators, such as U/Th, V/(V+Ni), and As/Al ratios that display a decreasing trend for the variegated sediments. In fact, the redox conditions have varied with time, as is shown by the redox indices for the green and red shales, respectively. Thin red shale layers in this series display the lowest values of the redox indices, suggestive of better oxygenation. Nevertheless, the whole series, except for the thin sediment directly overlying the Fe-Mn layer, is devoid of benthic microfossils and bioturbation, which seems to indicate stressed conditions at the basin floor. The values of the V/(V+Ni) ratio, especially in the green shales, suggest even dysoxia, taking into account the limit values proposed for such conditions by Hatch and Leventhal (1992). It is here hypothesized that the low oxygen content at the basin floor could be related to high temperatures of bottom waters, suggested for this period by Norris and Wilson (1998), Gustafsson *et al.* (2003), and Voigt *et al.* (2003). The sluggish bottom water circulation during the deposition of the organic-rich series, was certainly enhanced later, but there were pulses of high-velocity bottom currents which increased oxygen content at the basin floor, after which followed permanent and full oxygenation of bottom waters. Low values of the Ce/La ratio (2.1–2.5; Table 1) calculated for the sediments above the organic-rich facies, which are a proxy for the oxygen content in the water masses (Glasby *et al.*, 1997; Kunzendorf *et al.*, 1993; Kasten *et al.*, 1998), support this interpretation. The strongest and long-termed oxygenation of bottom water took place only at the beginning of the bottom water reorganisation, probably responsible for the diagenetic transformations of the first horizon of the Fe-Mn layer. It is here also confirmed by the occurrence of a 10-cm-thick succession of red shales, whose base is 30 cm above this Fe-Mn layer. Higher up, only very thin (a few mm thick) and dispersed red shale layers occur, demonstrating only short-termed impulses of bottom currents, transporting better oxygenated water masses. In contrast, sluggish circulation, associated with enhanced primary productivity caused the occurrence of even periodic anoxia, which resulted in deposition of two dark-laminated black shales, strongly enriched in marine organic matter. The high content of TOC in these shales can be here also attributed to the extremely low clastic supply caused by the high sea level stand. The well-oxygenated conditions at the basin floor, demonstrated by diversified foraminiferal agglutinated assemblages, appeared within the *Quadrum gartneri* calcareous nannoplankton Zone, corresponding to the Lower Turonian. The DWAF includes numerous infaunal morphotypes belonging to the *Uvigerinammina jankoi* assemblage, typical of Turonian–Lower Campanian red and variegated facies from the Western Tethyan abyssal and bathyal environments, formed in well-oxygenated conditions at basin floor (e.g., Kuhnt *et al.*, 1992; Bąk, K., 2000).

Changes in primary productivity during the C–T boundary interval

The presence of numerous radiolarian-rich layers above the organic-rich series may be interpreted as the record of a relatively high level of primary productivity in the Skole Basin, gently increasing up-section in comparison to the Late Cenomanian series. The radiolarian assemblages from the variegated shales consist mainly of small specimens of the genus *Holocryptocanium*, which probably could be regarded as an opportunistic form, related to the upwelling areas. A dominance of this genus was also observed in the organic-rich sequence and in the underlying hemipelagic shales within the calciturbidite succession. Accordingly, the numerous radiolarian-rich layers present in the whole studied section may reflect seasonal? upwelling circulation at the margin of the Carpathian Basin, suggested also by the data from the Subsilesian and Silesian nappes (Bąk K., 2006, 2007a).

Some chemical signals, like the content of silica and sedimentary barium, confirm the increase of primary productivity after the deposition of the organic-rich facies. However, the preservation and diagenetic remobilization of primary opaline and barium could restrict their application as a proxy for surface water productivity (e.g., Von Breymann *et al.*, 1990; Dymond *et al.*, 1992; Tribovillard *et al.*, 1996).

The negative correlation between Al_2O_3 and SiO_2 (Fig. 11B) for sediments overlying the first Fe-Mn layer may be explained by predominance of biogenic silica, diluted by terrigenous particles. In this sense, the high content of silica in the variegated shales, in comparison with the underlying series, may demonstrate a relative increase in productivity in latest Cenomanian–earliest Turonian times. However, the above mentioned trend could be also caused (at least partially) by decreasing terrigenous supply to the basin floor during the maximum of the worldwide transgression.

More questions concern the use of barium as a proxy for surface primary productivity, especially if the changes in Ba content are interpreted without knowledge of the particulate Ba phases. The presented data on the barium content are based only on the bulk sample composition, thus the content of Ba from sedimentary barite, Fe/Mn oxides and detritic Ba associated with aluminosilicates, is not known here. Furthermore, the effects of suboxic diagenesis may have influenced the Ba content in the studied sediments (McManus *et al.*, 1998, 1999). Consequently, the presented Ba/Al and Ba/Sc ratios may present only general trends in changes of primary productivity, as referred by Reitz *et al.* (2004). However, even this trend may not only reflect variations in primary productivity, but may also result from changes in supply of aluminosilicates and from changes in the type of lithogenic material delivered to the basin floor. The marginal position of the Skole Basin, close to the West European Platform, favoured supply of continental debris including aluminosilicate particles. In contrast, this supply decreased during the Late Cenomanian–Early Turonian progressive worldwide transgression.

The plot of Ba/Al shows a surprisingly high value in the first Fe-Mn layer. The origin of barium could be different here. The data from present-day sediments demonstrate that Ba could be scavenged immediately from seawater by Mn oxides (e.g., Keninson Falkner *et al.*, 1993; De Lange *et al.*, 1990, 1994) but it also may have coprecipitated within newly formed Mn oxides during early diagenesis (e.g., Kumar *et al.*, 1996; Schroeder *et al.*, 1997). In the latter case, Ba^{2+} is released into pore-water by barite dissolution and scavenged by Mn oxides in the oxic zone of the sediment. Barite could here originate from the cement within the primary Fe-Mn carbonates. Such associations are known from authigenic Fe-Mn carbonates in deep-water marine sediments (e.g., in the Cenozoic silts and clays of the Arctic Ocean and the Norwegian-Greenland Sea, Sites 909 and 911; Chow *et al.*, 2000). The high concentration of Ba in the Mn oxides (ca. 6500 ppm) in the studied Fe-Mn layer is 300% higher than that reported from the Pacific and Atlantic Oceans, where the Ba content in the Mn oxide-hydroxides ranges between 1000 and 2000 ppm (Dymond *et al.*, 1992). However, in well-oxygenated sediments in the Arabian Sea, Ba content in Mn oxides attains even 6000 ppm (Schenau *et al.*, 2001), similarly as in the studied Fe-Mn layer.

The plots of Ba/Al and Ba/Sc ratios in hemipelagic shales show significantly higher values in the variegated sediments than in the underlying series (Fig. 13). These values, similar to the mean value determined for the CTBE by Warning and Brumsack (2000), are even 200% higher than in the uppermost Cenomanian calciturbidite series. Accordingly, irrespective of the discussed above restrictions in application of Ba/Al and Ba/Sc ratios as the productivity proxy, it seems that surface waters were under influence of seasonal? coastal upwelling during the earliest Turonian, which resulted in increased primary productivity in the marginal part of the Carpathian Basin.

CONCLUSIONS

1. Microfacies, microfossils and chemical data allowed the recognition of the oceanic anoxic event (OAE-2) in the previously undifferentiated Cenomanian–Turonian succession in the Skole Nappe of the Polish Outer Carpathians.

2. The OAE-2 was preceded in the Skole Basin by sedimentation of diluted gravity flows transporting mainly biogenic material from the shelves of the West European Platform. This sedimentary record was concurrent with spicule-rich turbidite sedimentation, in another marginal basin of the Outer Carpathians, the Silesian Basin. In both basins, the biogenic-rich-turbidite sedimentation gradually disappeared during the latest Cenomanian (near the beginning of the $\delta^{13}C$ excursion), being related to the ongoing eustatic rise and the expansion of the oxygen minimum zone.

3. The uppermost Cenomanian organic-rich facies (Bonarelli-equivallent horizon) records the OAE-2. The benthos-free black sediments, characterized by positive excursions of chemical redox indices, are indicative of bottom water anoxia, interrupted by intervals of suboxic conditions, expressed by the sedimentation of hemipelagic green shales. These sediments contain a low number of poorly-diversified deep-water agglutinated foraminifers, which represent a stressed assemblage of the so-called "Biofacies B", related to oxygen-depleted conditions coinciding probably with the increasing temperature of bottom water.

4. The ferromanganese layer, covered by a 70 cm thick succession of siliceous-manganiferous shales, directly overlies the organic-rich facies. These sediments have been deposited under well-oxygenated bottom- and pore-water related to an increase in deep-water circulation.

5. Increasing, but not permanent, oxygenation of bottom waters is suggested for the lowermost Turonian variegated shales. Negative excursions of chemical redox indices like U/Th, V/(V+Ni), and As/Al ratios, indicate better oxygenation, but low values of the Ce/La ratio and the lack of benthos and bioturbation point to predominance of sluggish circulation and stressed conditions at the basin floor, with pulses of high-velocity bottom currents that increased the oxygen content near the basin floor. Occasionally, sluggish circulation, associated with enhanced primary productivity, resulted in bottom water anoxia, marked by the deposition of organic-rich black shales. The well-oxygenated conditions at the basin floor, demonstrated by diversified foraminiferal agglutinated assemblages, appeared in the Early Turonian, corresponding to the calcareous nannoplankton *Quadrum gartneri* Zone.

8. A high frequency of radiolarian-rich layers above the Bonarelli-equivalent horizon and the increase in Ba/Al and Ba/Sc ratios are interpreted as the result of a relatively high level of primary productivity in the Skole Basin, gently increasing up-section in comparison to the Upper Cenomanian successions.

Acknowledgements

Anna Łatkiewicz and Jadwiga Faber (Jagiellonian University) are gratefully acknowledged for performing the X-ray diffraction determinations, help in electron microprobe point analyses and SEM micrographs. Andrzej and Jarosław Szumny (AGH University of Science and Technology, Kraków) are acknowledged for preparation of thin sections. Malcolm Hart (University of Plymouth, U. K.), Mike Kaminski (University College London), Grzegorz Haczewski (Świętokrzyska Academy), Michał Krobicki (AGH University of Science and Technology, Kraków) and anonymous reviewers are thanked for comments on the manuscript and improving the English. This work was supported by the Polish Committee for Scientific Research grant AP-IG/49/ 2004–2006.

REFERENCES

Amorosi, A., 1997. Detecting compositional, spatial, and temporal attributes of glaucony: a tool for provenance research. *Sedimentary Geology*, 109: 135–153.

Arthur, M. A., 1979. North Atlantic Cretaceous black shales: The record at Site 398 and brief comparison with other occurrences. In: Sibuet, J. C., Ryan, W. B. F. (eds), *Initial Reports*

of the Deep Sea Drilling Program, 47, pp. 719–752.

Arthur, M. A. & Premoli Silva, I., 1982. Development of widespread organic carbon-rich strata in the Mediterranean Tethys. In: Schlanger, S. O., Cita, M. B. (eds), *Nature and Origin of Cretaceous Carbon-Rich Facies*, Academic Press, London, pp. 7–54.

Bąk, K., 2000. Biostratigraphy of deep-water agglutinated Foraminifera in Scaglia Rossa-type deposits of the Pieniny Klippen Belt, Carpathians, Poland. In: Hart, M. B., Kaminski, M. A. & Smart, C. (eds), *Proceedings of the Fifth International Workshop on Agglutinated Foraminifera, Plymouth, England, September 12-19, 1997, Grzybowski Found. Special Publication*, 7, pp. 15–41.

Bąk, K., 2006. Sedimentological, geochemical and microfaunal responses to environmental changes around the Cenomanian–Turonian boundary in the Outer Carpathian Basin; a record from the Subsilesian Nappe, Poland. *Palaeogeography, Palaeoecology, Palaeoclimatology*, 237: 335–358.

Bąk, K., 2007a. Deep-water facies succession around the Cenomanian–Turonian boundary in the Outer Carpathian Basin: high-resolution sedimentary, biotic and chemical records in the Silesian Nappe, Poland. Submitted to *Palaeogeography, Palaeoecology, Palaeoclimatology*. Doi: 101016/j.palaeo. 2006.12.005.

Bąk, K., 2007b. Organic-rich and manganese sedimentation during the Cenomanian–Turonian boundary event in the Outer Carpathian Basin; a new record from the Skole Nappe, Poland, and a review from other tectonic units. Submitted to *Palaeogeography, Palaeoecology, Palaeoclimatology*.

Bąk, K., Bąk, M. & Paul, Z., 2001. Barnasiówka Radiolarian Shale Formation – a new lithostratigraphic unit in the Upper Cenomanian – lowermost Turonian of the Polish Outer Carpathians (Silesian Series). *Annales Societatis Geologorum Poloniae*, 71: 75–103.

Bąk, K., Bąk, M. & Gaździcka, E., 2005. High resolution radiolarian, foraminiferal and calcareous nannoplankton biostratigraphy of the Upper Cenomanian–Lower Turonian deep-water sediments in the Polish Outer Carpathians. In: Godet, A., Mort, H., Linder, P. & Bodin, S. (eds), *7th International Symposium on the Cretaceous, 5–9 Sept. 2005, Neuchatel, Scientific Program and Abstracts*, p. 43.

Bąk, M., 2000. Radiolaria from the Upper Cenomanian–Lower Turonian deposits of the Silesian Unit (Polish Flysch Carpathians). *Geologica Carpathica*, 51: 309–324.

Bąk, M., 2004. Radiolarian biostratigraphy of the Upper Cenomanian–Lower Turonian deposits in the Subsilesian Nappe (Outer Western Carpathians). *Geologica Carpathica*, 55: 239–250.

Bąk, M., Bąk, K. & Ciurej, A., 2005. Mid-Cretaceous spicule-rich turbidites in the Silesian Nappe of the Polish Outer Carpathians: radiolarian and foraminiferal biostratigraphy. *Geological Quarterly*, 49: 275–290.

Bengston, P., 1996. The Turonian stage and substage boundaries. *Bulletin de l'Institut Royal des Sciences Naturelles de Belgique*, 66: 69–79.

Bralower, T. J. & Thierstein, H. R., 1984. Low productivity and slow deep-water circulation in mid-Cretaceous oceans. *Geology*, 12: 614–618.

Burtanówna, J., 1933. Der geologische Bau der Umgegend von Myślenice westlisch vom Raba-Fluss. *Annales de la Société Géologique de Pologne*, 9: 279–293.

Caron, M., Dall'Agnollo, S., Accarie, H., Barrera, E., Kauffman, E. G., Amédro, F. & Robaszynski, F., 2006. High resolution stratigraphy of the Cenomanian–Turonian boundary interval at Pueblo (USA) and Wadi Bahlul (Tunisia): stable isotope and bio-events correlation. *Geobios*, 39: 171–200.

Chow, N., Morad, S. & Al-Aasm, I. S., 2000. Origin of authigenic Mn-Fe carbonates and pore-water evolution in marine sediments; evidence from Cenozoic strata of the Arctic Ocean and Norwegian-Greenland Sea (ODP Leg 151). *Journal of Sedimentary Research*, 70: 682–699.

Dehairs, F., Chesselet, R. & Jedwab, J., 1980. Discrete suspended particles of barite and the barium cycle in the open ocean. *Earth Planetary Science Letters*, 49: 528–550.

De Lange, G. J., Catalano, G., Klinkhammer, G. P. & Luther III G. W., 1990. The interface between oxic seawater and the anoxic Banock brine; its sharpness and the cosequences for the redox-related cycling of manganese and barium. *Marine Chemistry*, 31: 205–217.

De Lange, G. J., Van Os, B., Pruysers, P. A., Middelbourg, J. J., Castradori, D., Van Santvoort, P., Muller, P. J., Eggenkamp, H. & Prahl, F. G., 1994. Possible early diagenetic alteration of palaeo proxies. In: Zahn, M. A. *et al.* (eds), *Carbon Cycling in the Glacial Ocean: Constraints on the Oceans's Role in Global Change, NATO ASI Series* 1, 17, pp. 225–258.

Dickens, G. R. & Owen, R. M., 1996. Sediment geochemical evidence for an early–middle Gilbert (early Pliocene) productivity peak in the North Pacific Red Clay Province. *Marine Micropaleontology*, 27: 107–120.

Dymond, J., Suess, E. & Lyle, M., 1992. Barium in deep-sea sediment: a proxy for paleoproductivity. *Paleoceanography*, 7: 163–181.

Erba, 2004. Calcareous nannofossils and Mesozoic oceanic events. *Marine Micropaleontology*, 52: 85–106.

Farmer, J. G. & Lovell, M. A., 1986. Natural enrichment of arsenic in Loch Lomond sediments. *Geochimica et Cosmochimica Acta*, 50: 2059–2067.

Ferguson, J. F. & Gavis, J., 1972. A review of the arsenic cycle in natural waters. *Water Resources*, 6: 1259–1274.

Francesconi, K. A. & Edmonds, J. S., 1998. Arsenic species in marine samples. *Croatica Chemica Acta*, 71: 342–359.

Gawor-Biedowa, E., 1972. The Albian, Cenomanian and Turonian foraminifers of Poland and their stratigraphic importance. *Acta Paleontologica Polonica*, 17: 3–165.

Glasby, G. P., Stüben, D., Jeschke, G., Stoffers, P. & Garbe-Schönberg, C.-D., 1997. A model for the formation of hydrothermal manganese crusts from the Pitcairn Island hotspot. *Geochimica et Cosmochimica Acta*, 61: 4583–4597.

Golonka, J., Oszczypko, N. & Ślączka, A., 2000. Late Carboniferous–Neogene geodynamic evolution and palaeogeography of the circum-Carpathian region and adjacent areas. *Annales Societatis Geologorum Poloniae*, 70: 107–136.

Golonka, J. & Krobicki, M., 2001. Upwelling regime in the Carpathian Tethys: a Jurassic – Cretaceous palaeogeographic and palaeoclimatic perspective. *Geological Quarterly*, 45: 15–32.

Gradstein, F. M., Ogg, J. G., Smith, A. G. *et al.*, 2004. *A Geologic Time Scale 2004*. Cambridge University Press.

Gräfe, K.-U., 2005. Late Cretaceous benthic foraminifers from Basque-Cantabrian Basin, Northern Spain. *Iberian Geology*, 31: 277–298.

Gucik, S., 1987. *Explanations to the Detailed Geological Map of Poland, scale 1:50,000; Krzywcza (1026) Sheet*. [In Polish]. Wydawnictwa Geologiczne, Warszawa.

Gucik, S., Jankowski, L., Rączkowski, W. & Żytko, K., 1991. *Explanations to the Detailed Geological Map of Poland, scale 1:50,000; Rybotycze (1043) and Dobromil (1044) Sheets*. [In

Polish]. Wydawnictwa Geologiczne, Warszawa.

Gucwa, I., 1966. Results of geochemical examinations of radiolarian shales from Niedźwiada, near Ropczyce. [In Polish, English summary]. *Kwartalnik Geologiczny*, 10: 1047–1059.

Gustafsson, M., Holbourn, A. & Kuhnt, W., 2003. Changes in Northeast Atlantic temperature and carbon flux during the Cenomanian/Turonian paleoceanographic event: the Goban Spur stable isotope record. *Palaeogeography, Palaeoecology, Palaeoclimatology*, 201: 51–66.

Hart, M. B. & Swiecicki, A., 1988. The genus *Gavelinella* Brotzen, 1942, in the Cretaceous strata of the U.K. *Revue Paléobiology*, Vol. Spéc., 2: 289–294.

Hatch, J. R. & Leventhal, J. S., 1992. Relationship between inferred redox potential of the depositional environment and geochemistry of the Upper Pensylvanian (Missourian) Stark Shale Member of the Dennis Limestone, Wabaunsee County, KS, U.S.A. *Chemical Geology*, 99: 65–82.

Heller, I, 1975. Microbiostratigraphy of the Cretaceous deposits in the southern part of the Łódź Synklinorium (Central Poland). *Annales Societatis Geologorum Poloniae*, 55: 233–254.

Herbin, J. P., Montadert, L., Muller, C., Gomez, R., Thurow, J. & Wiedmann, J., 1986. Organic-rich sedimentation at the Cenomanian–Turonian boundary in oceanic and coastal basins in the North Atlantic and Tethys. In: Summerhayes, C. P. & Shackleton, N. J. (eds), *North Atlantic Palaeoceanography*, Geological Society, London, Special Publication, 21, pp. 389–422.

Herbin, J. P., Moullade, M., Brumsack, H.-J., Masure, E., Taugourdeau-Lantz, J. & Dunham, K., 1988. The Cenomanian/Turonian Boundary Event at Hole 641A, ODP Leg 103 (compared with the CTBE Intreval at Site 398). In: Boillot, G., Witerer, E.L. *et al.* (eds), *Proceedings of the Ocean Drilling Program, Scientific Results*, 103, pp. 587–634.

Hradecka, L., 1993. *Gavelinella* Brotzen, 1942 and *Lingulogavelinella* Malapris, 1969 (Foraminifera) from the Bohemian Basin. *Sbornik Geologickych Ved*, *Paleontologia*, Praha, 33: 79–96.

Hradecka, L. & Švábenickà, L., 1995. Foraminifera and calcareous nannoplankton assemblages from the Cenomanian – Turonian boundary interval of the Knoviz section, Bohemian Cretaceous Basin. *Geologica Carpathica*, 46: 267–276.

Jacquin, T. & Graciansky, P. C. de, 1998. Major transgressive/regressive cycles: the stratigraphic signature of European Basin development. In: Graciansky, P. C. de *et al.* (eds), Mesozoic *and Cenozoic Sequence Stratigraphy of European Basins*. SEPM Special Publication, Tulsa, 60, pp. 15–29.

Jenkyns, H. C., 1980. Cretaceous anoxic events: from continents to oceans. *Journal of Geological Society, London*, 137: 171–188.

Jones, B. & Manning, D. A. C., 1994. Comparison of geochemical indices used for the interpretation of paleoredox conditions in ancient mudstones. *Chemical Geology*, 111: 111–129.

Kasten, S., Glasby, G. P., Schulz, H. D., Friedrich, G. & Andreev, S. I., 1998. Rare earth elements in manganese nodules from the South Atlantic Ocean as indicators of oceanic bottom water flow. *Marine Geology*, 146: 33–52.

Keller, G., Berener, Z., Adatte, T. & Stueben, D., 2004. Cenomanian–Turonian and $\delta^{13}C$, and $\delta^{18}O$, sea level and salinity variations at Pueblo, Colorado. *Palaeogeography, Palaeoecology, Palaeoclimatology*, 211: 19–43.

Keninson Falkner, K., Klinkhammer, G. P., Bowers, T. S., Todd, J. F., Lewis, B. L., Landing, W. M. & Edmond, J. M., 1993. The behavior of barium in anoxic marine waters. *Geochimica et Cosmochimica Acta*, 57: 537–554.

Koszarski, L. & Morgiel, J., 1963. Initial research on the Cretaceous biostratigraphy in the Skole Unit near Tarnów. [In Polish]. *Kwartalnik Geologiczny*, 7: 555–557.

Koszarski, L. & Ślączka, A., 1973. Outer (flysch) Carpathians: Lower Cretaceous. In: Pożaryski, W. (ed.), *Geology of Poland*, Wydawnictwa Geologiczne, Warszawa, pp. 492–495.

Kotlarczyk, J., 1978. Stratigraphy of the Ropianka Formation or of Inoceramian Beds in the Skole Unit of the Flysch Carpathians. [In Polish, English summary]. *Prace Geologiczne PAN – Oddział w Krakowie*, 108: 1–82.

Książkiewicz, M. (ed.), 1962. *Geological Atlas of Poland; Stratigraphic and facial problems*, vol. 13. *Cretaceous and Older Paleogene in the Polish Outer Carpathians*. Instytut Geologiczny, Wydawnictwa Geologiczne, Warszawa, 20 maps, 20 pp. explanatory notes.

Kuhnt, W. & Kaminski, M. A., 1989. Upper Cretaceous deep-water agglutinated benthic foraminiferal assemblages from the Western Mediterranean and adjacent areas. In: Wiedmann, J. (ed.), *Cretaceous of the Western Tethys. Proceedings of 3rd International Cretaceous Symposium*, Stuttgart (Schweizerbart), pp. 93–120.

Kuhnt, W., Herbin, J. P., Thurow, J. & Wiedmann, J., 1990. Distribution of Cenomanian–Turonian organic facies in the western Mediterranean and along the adjacent Atlantic margin. In: Huc, A.Y. (ed.), *Deposition of organic facies. American Association of Petroleum Geologists Bulletin*, 30: 133–160.

Kuhnt, W., Geroch, S., Kaminski, M. A., Moullade, M. & Neagu, T., 1992. Upper Cretaceous abyssal claystones in the North Atlantic and Western Tethys: current status of biostratigraphical correlation using agglutinated foraminifers and palaeoceanographic events. *Cretaceous Research*, 13: 467– 478.

Kuhnt, W., Luderer, F., Nederbragt, S., Thurow, J. & Wagner, T., 2005. Orbital-scale record of the late Cenomanian–Turonian oceanic anoxic event (OAE-2) in the Tarfaya Basin (Morocco). *International Journal of Earth Sciences*, 94: 147–159.

Kumar, N., Anderson, R. F. & Biscayae, P. E., 1996. Remineralization of particulate authigenic trace metals in the Middle Atlantic Bight: Implications for proxies of export productivity. *Geochimica et Cosmochimica Acta*, 60: 3383–3397.

Kunzendorf, H., Glasby, G. P., Stoffers, P. & Pluger, W. L., 1993. The distribution of rare elements and minor elements in manganese nodules, micronodules and sediments along an east-west transect in the southern Pacific. *Lithos*, 30, 45–56.

Leckie, R. M., Bralower, T. J. & Cashman, R., 2002. Oceanic anoxic events and plankton evolution: biotic response to tectonic forcing during mid-Cretaceous. *Paleoceanography*, 17: 1041 (10.1029/2001PA000623).

Luciani, V. & Cobianchi, M., 1999. The Bonarelli Level and other black shales in the Cenomanian–Turonian of the northeastern Dolomites (Italy): calcareous nannofossil and foraminiferal data. *Cretaceous Research*, 20: 135–167.

Lüning, S., Kolonic, S., Belhadj, E. M., Belhadj, Z., Cota, L., Barić, G. & Wagner, T., 2004. Integrated depositional model for the Cenomanian–Turonian organic-rich strata in North Africa. *Earth Sciences Review*, 64: 51–117.

Machhlour, L., Philip, J. & Oudin, J. L., 1994. Formation of laminate deposits in anaerobic – dysaerobic marine environments. *Marine Geology*, 117: 287–302.

Masuzawa, T., 1989. Compositional change of settling particles with water depth in the Japan Sea. *Marine Chemistry*, 27: 61–78.

McManus, J., Berelson, W. M., Klinkhammer, G. P., Johnson, K. S., Coale, K. H., Anderson, R. F., Kumar, N., Burdige, D. J., Hammond, D. E., Brumsack, H. J., McCorkle, D. C. & Rushdi, A., 1998. Geochemistry of barium in marine sediments: Implications for its use as a paleoproxy. *Geochimica et Cosmochimica Acta*, 62: 3453–3473.

McManus, J., Berelson, W. M., Hammond, D. E. & Klinkhammer, G. P., 1999. Barium cycling in the north Pacific: Implications for the utility of Ba as a paleoproductivity and a paleoalkalinity proxy. *Paleoceanography*, 14: 53–61.

McRae, S. G., 1972. Glauconite. *Earth Science Review*, 8: 397–440.

Minami, H. & Kato, Y., 1997. Remobilization of arsenic in suboxic sediments from the seafloor of the continental margin. *Journal of Oceanography*, 53: 553–562.

Norris, R. D., Wilson, P. A., 1998. Low latitude sea-surface temperatures for the mid-Cretaceous and the evolution of planktonic foraminifera: comment and reply. *Geology*, 27: 858.

Oszczypko, N., 2004. The structural position and tectonosedimentary evolution of the Polish Outer Carpathians. *Przegląd Geologiczny*, 52: 780–791.

Paul, C. R. C., Lamolda, M. A., Mitchel S. F., Vaziri, M. R., Gorostidi, A. & Marshall, J. D., 1999. The Cenomanian–Turonian boundary at Eastbourne (Sussex, UK): a proposed European reference section. *Palaeogeography, Palaeoecology, Palaeoclimatology*, 150: 83–121.

Pedersen, T. F. & Calvert, S. E., 1990. Anoxia vs. productivity: what controls the formation of organic carbon-rich sediments and sedimentary rocks? *American Association of Petroleum Geologists, Bulletin*, 74: 454–466.

Peryt, D. 1983. Mid-Cretaceous microbiostratigraphy and foraminifers of the NE margins of the Świętokrzyskie (Holy Cross) Mts., Poland. *Acta Paleontologica Polonica*, 28: 417–466.

Peryt, D. & Wyrwicka, K., 1991. The Cenomanian–Turonian oceanic anoxic event in SE Poland. *Cretaceous Research*, 12: 65–80.

Peryt, D. & Wyrwicka, K., 1993. The Cenomanian/Turonian boundary event in Central Poland. *Palaeogeography, Palaeoecology, Palaeoclimatology*, 104: 185–197.

Poprawa, D. & Nemčok, J. (eds), 1998. *Geological Atlas of the Outer Carpathians and Their Foreland 1:500,000*. Państwowy Instytut Geologiczny, Warszawa.

Pratt, L. M. & Threlkeld, C. N., 1984. Stratigraphic significance of $^{13}C/^{12}C$ ratios in mid-Cretaceous rocks of theWestern Interior, USA. In: Stott, D. F. & Glass, D. J. (eds), *The Mesozoic of Middle North America. Canadian Society Petroleum Geological Memoirs*, 9, pp. 305–312.

Rantisch, G., Melcher, F., Meisel, T. & Rainer, T., 2003. Rare elements, major and trace elements in Jurassic manganese shales of the Northern Calcareous Alps: hydrothermal versus hydrogenous origin of stratiform manganese deposits. *Mineralogy and Petrology*, 77: 109–127.

Reitz, A., Pfeifer, K., de Lange, G. J. & Klump, J., 2004. Biogenic barium and the detrital Ba/Al ratio: a comparison of their direct and indirect determination. *Marine Geology*, 204: 289–300.

Sageman, B. B., Meyers, S. R. & Arthur, M. A., 2006. Orbital time scale and new C-isotope record for Cenomanian–Turonian boundary stratotype. *Geology*. 34: 125–128.

Schenau, S. J., Prins, M. A., De Lange, G. J. & Monnin, C., 2001. Barium accumulation in the Arabian Sea: controls on barite preservation in marine sediments. *Geochimica et Cosmochimica Acta*, 65: 1545–1556.

Schlanger, S. O., Jenkyns, H. C., 1976. Cretaceous oceanic anoxic events, causes and consequences. *Geologie et Mijnbow*, 55: 179–184.

Schroeder, J. O., Murray, R. W., Leinen, M., Pflaum, R. C. & Janecek, T. R., 1997. Barium in equatorial Pacific carbonate sediment: Terrigenous, oxide, and biogenic associations. *Paleoceanography*, 12:125–146.

Scopelliti, G., Bellanca, A., Coccioni, R., Luciani, V., Neria, R., Baudin, F., Chiari, M. & Marcucci, M., 2004. High-resolution geochemical and biotic records of the Tethyan 'Bonarelli Level' (OAE2, latest Cenomanian) from the Calabianca–Guidaloca composite section, northwestern Sicily, Italy. *Palaeogeography, Palaeoecology, Palaeoclimatology*, 208: 293–317.

Sinninghe Damsté, J. A. & Köster, J., 1998. A euxinic southern North Atlantic Ocean during the Cenomanian/Turonian oceanic anoxic event. *Earth Planetary Science Letters*, 158: 165–173.

Sujkowski, Z., 1932. Radiolarites des Karpates Polonaises Orientales et leur comparaison avec les Radiolarites de la Tatra. Étude lithologique. [In Polish, French summary]. *Bulletine Service Geologique Pologne* (*Varsovie*), 7: 97–168.

Summerhayes, C. P., 1981. Organic facies of Middle Cretaceous black shales in deep North Atlantic. *American Association of Petroleum Geologist, Bulletin*, 65: 2364–2380.

Ślączka, A. & Kaminski, M. A., 1998. *Guidebook to Excursions in the Polish Flysch Carpathians*. Grzybowski Found. Special Publication, 6, 171 pp.

Tribovillard, N.-P., Caulet, J.-P., Vergnaud-Grazzini, C., Moureau, N. & Tremblay, P., 1996. Lack of organic matter accumulation on the upwelling-influenced Somalia margin in a glacial-interglacial transition. *Marine Geology*, 133: 157–182.

Tsikos, H, Jenkyns, H. C., Walsworth-Bell, B. & Petrizzo, M. R., 2004. Carbon-isotope stratigraphy recorded by the Cenomanian–Turonian Oceanic Anoxic Event: correlation and implications based on three key localities. *Journal of Geological Society, London*, 161: 711–719.

Tyson, R. V., 1995. *Sedimentary Organic Matter: Organic Facies and Palynofacies*. Chapman and Hall, London, 615 pp.

Van Os, B. J. H., Middelburg, J. J. & de Lange, G. J., 1991. Possible diagenetic mobilization of barium in sapropelic sediments from the eastern Mediterranean. *Marine Geology*, 100: 125–136.

Von Breymann, M. T., Emeis, K. C. & Camerlenghi, A., 1990. Geochemistry of sediments from the Peru upwelling area: Results from sites 680, 682, 685, and 688. *Proceedings of the Ocean Drilling Program, Scientific Results*, 112: 491–503.

Voigt, S., Wilmsen, M., Mortimore, R. N. & Voigt, T., 2003. Cenomanian palaeotemperatures derived from the oxygen isotopic composition of brachiopods and belemnites: evaluation of Cretaceous palaeotemperature proxies. *International Journal of Earth Sciences*, 92: 285–299.

Wehausen, R. & Brumsack, H.-J., 1998. The formation of Pliocene Mediterranean sapropels: constraints from high-resolution major and minor element studies. In: Robertson, A. H. F., Emeis, K.-C., Richter, C. *et al.* (eds), *Proceedings of the Ocean Drilling Program, Scientific Results*, 160, College Station, TX, pp. 207–217.

Warning, B. & Brumsack, H.-J., 2000. Trace metal signatures of Mediterranean sapropels. *Palaeogeography, Palaeoecology, Palaeoclimatology*, 158: 293–309.

Wójcik-Tabol, P., 2006. Organic carbon accumulation events in the mid-Cretaceous rocks of the Pieniny Klippen Belt (Polish Carpathians) – a petrological and geochemical approach. *Geological Quarterly*, 50: 419–436.

Zhurakovsky, A. G., 1968. Certain new data on the Cretaceous deposits of the Striy river bassins. [In Russian, English summary]. *Geologichznyj Sbornik* (*Lvov*) 11: 36–42.

Streszczenie

ZMIANY W GŁĘBOKOWODNYM ŚRODOWISKU BRZEŻNEJ CZĘŚCI BASENU KARPAT ZEWNĘTRZNYCH WOKÓŁ GRANICY CENOMANU I TURONU WYRAŻONE W ZAPISIE MIKROFACJI, ZESPOŁACH MIKROSKAMIENIAŁOŚCI I CHEMIŹMIE UTWORÓW W PŁASZCZOWINIE SKOLSKIEJ

Krzysztof Bąk

Anoksyczne zdarzenie oceaniczne z granicy cenomanu i turonu, odzwierciedlone przez sedymentację czarnych łupków organicznych i łupków radiolariowych (tzw. CTBE, OAE-2, Bonarelli Event) było przedmiotem licznych i wielokierunkowych badań pod kątem określenia jego cech, przyczyn i skutków, jakie spowodowało (np., Arthur, 1979; Jenkyns, 1980; Summerhayes, 1981; Arthur & Premoli Silva, 1982; Bralower & Thierstein, 1984; Herbin *et al*., 1986; Kuhnt *et al*., 1990; Pedersen & Calvert, 1990; Peryt & Wyrwicka, 1991, 1993; Tyson, 1995; Sinninghe Damsté & Köster, 1998; Gustafsson *et al.*, 2003; Lüning *et al*, 2004; Kuhnt *et al*., 2005; Wójcik-Tabol, 2006). Zapis tego zdarzenia jest znany głównie ze środowisk mórz epikontynentalnych i obszarów oceanicznych z sedymentacją węglanową. Profile osadów cenomanu i turonu z basenów głębokowodnych, z dnem poniżej granicy kompensacji węglanowej są nieliczne i natura tego zdarzenia jest słabo poznana z takich środowisk. W niniejszej pracy przedstawiono zapis anoksycznego zdarzenia oceanicznego na granicy cenomanu i turonu w głębokowodnym basenie Karpat Zewnętrznych, wraz z interpretacją zmian, jakie zaszły na dnie tego basenu. Artykuł ten jest uzupełnieniem serii badań autora na ww. temat, opublikowanych wcześniej w oparciu o profile z dwóch innych jednostek tektonicznych Karpat Zewnętrznych (Bąk K., 2006, 2007a).

Prezentowane badania były oparte o zmienność facji, skład chemiczny utworów hemipelagicznych oraz zmienność zespołów otwornic aglutynujących. Osady badanego profilu ("profilu Spława") były deponowane w brzeżnej części basenu Karpat Zewnętrznych, w tzw. basenie skolskim (Fig. 1A). Głównym celem pracy była interpretacja zmian zawartości tlenu w wodach dennych tej części basenu Karpat, interpretacja zmian produktywności wód powierzchniowych oraz interpretacja zmian w dostawie materiału okruchowego do dna basenu w czasie od późnego cenomanu do wczesnego turonu. Zmiany powyższych parametrów środowiska basenu skolskiego zostały skorelowane z danymi biostratygraficznymi i chemostratygraficznymi, analizowanymi wcześniej przez autora w tym samym profilu (Bąk K., 2007b).

Badany profil znajduje się w centralnej części jednostki skolskiej w obrębie antykliny Grunowej – Spławy, na dwóch brzegach potoku Krzeczkowskiego, na północ od wzgórza Spława, około 25 km na SW od Przemyśla (Fig. 1B–D). Seria badanych osadów w tym profilu obejmuje środkową i górną część formacji łupków radiolariowych z Barnasiówki (ŁRB) oraz najniższą część sukcesji pstrych łupków (Fig. 2, 3). Formacja ŁRB obejmuje na tym obszarze: 1) zielone bezwapniste łupki (niebędące tutaj przedmiotem badań), 2) cienkoławicowe margle krzemionkowe z zielonymi i czarnymi łupkami bezwapnistymi (przynajmniej 20 m miąższości), 3) serię łupków organicznych z bentonitami, stanowiącą horyzont o maksymalnej zawartości materii organicznej (ok. 1,7 m miąższości), 4) pierwszy poziom żelazisto-manganowy (do 3 cm), 5) pstre łupki krzemionkowo-manganowe z drugim poziomem Fe-Mn w stropie wraz z podścielającym go poziomem łupku organicznego (0,7 m miąższości). Seria nadległych pstrych łupków jest stektonizowana. Przedmiotem badań były dwa pakiety tej jednostki o miąższościach ok. 4,0 i 1,2 m; pierwszy z nich leży zgodnie na formacji ŁRB (Fig. 3).

Dane biostratygraficzne oparte na zespołach otwornic i promienic z tego profilu (Bąk K. *et al*., 2005; Bąk K., 2007b) wskazują, że seria margli krzemionkowych (prawdopodobnie bez jej najniższej części) oraz łupków organicznych, korelowanych z poziomem "Bonarelli", odpowiada dolnej części poziomu *Whiteinella archaeocretacea* (Fig. 3). Z kolei analizy stałych izotopów węgla z materii organicznej wskazują, że sedymentacja czarnych łupków organicznych, miała miejsce w czasie bliskim momentowi znacznego wzrostu wartości $\delta^{13}C$, który był zdarzeniem o znaczeniu globalnym. W oparciu o graficzną korelację krzywych wartości $\delta^{13}C$ w profilu Spława z innymi profilami z Karpat Zewnętrznych (Bąk K., 2007b) oraz ich kalibrację z krzywą czasu orbitalnego w profilu stratotypowym granicy cenomanu i turonu (c/t) w Pueblo (Kolorado, USA; Sageman *et al*., 2006) możliwe było wskazanie czasu początku depozycji facji organicznych na ok. 430 tys. lat przed granicą c/t (szczegóły kalibracji – Bąk K., 2007a, b). Zakończenie sedymentacji czarnych łupków organicznych miało miejsce około 30–50 tys. lat przed granicą c/t jak wynika z powyższej kalibracji krzywych izotopowych. Z kolei powstanie warstwy Fe-Mn wraz z sedymentacją serii pstrych łupków krzemionkowo-manganowych o miąższości 60 cm trwało przynajmniej 330–350 tys. lat. Czas sedymentacji drugiego poziomu Fe-Mn oraz nadległych pstrych łupków jest niemożliwy do określenia w oparciu o dane izotopowe. Obecność gatunku otwornicy aglutynującej *Uvigerinammina jankoi* i gatunku wapiennego nanoplanktonu *Quadrum gartneri* w drugim (wyższym) pakiecie pstrych łupków (Gaździcka w: Bąk K. *et al*., 2005) wskazuje, że ta część profilu osadów może korespondować z dolnym turonem.

W badaniach mikrofacji, składu chemicznego łupków hemipelagicznych oraz zespołów otwornic aglutynujących w łupkach wykorzystano ogółem 79 próbek skał pobranych w profilu o sumarycznej miąższości ok. 15 m (Fig. 3), przy czym mikrofacje były analizowane w 46 próbach, skład chemiczny łupków – w 45 próbach, a zespoły otwornic – w 47 próbach.

Seria cienkoławicowych margli i łupków marglistych, która stanowi najniższą część badanego profilu (ok. 6,5 m miąższości) to sukcesja cienkich turbidytów wapiennych (2–20 mm; Fig. 4A–C), gdzie granice warstw nie mają charakteru granic sedymentacyjnych, ale są efektem procesów diagenetycznych. Większość tych turbidytów to laminowane równolegle ziarnity, o zróżnicowanym składzie petrograficznym, głównie z ziarnami pochodzenia biogenicznego (Fig. 4D), przechodzące ku górze w waki wapienne, zawierające pokruszone szkielety otwornic, głównie planktonicznych (Fig. 4E). Otwornice planktoniczne, które są liczne również w ziarnitach należą do rodzaju *Hedbergella*, *Globigerinelloides*, *Heterohelix* i ?*Whiteinella* (Fig. 5A–D). Otwornice planktoniczne "z kilem" (?*Praeglobotruncana*, ?*Rotalipora*; Fig. 5E) występują jedynie w najniższej części badanej sukcesji margli

turbidytowych (Fig. 3). Niektóre z turbidytów wapiennych są wykształcone jako mikrytowe ziarnity, zawierające dużą liczbę igieł gąbek (Fig. 4F) oraz wapienne otwornice bentosowe należące do gavelinelidów (Fig. 5F–J), a także do rodzajów: *Gyroidinoides* (Fig. 5K, L), *Lenticulina* (Fig. 5M, N, R), ?*Nodosaria* (Fig. 5O) i *Dentalina* (Fig. 5P). W najwyższej części tej sukcesji, w obrębie wak wapiennych, występują liczne szkielety promienic, zdominowane przez rodzaj ?*Holocryptocanium* (Fig. 4G), lokalnie wymieszane z igłami gąbek (Fig. 5S). Igły gąbek należą do gromady Hexactinelidae (Fig. 6B–D) i Demospongiae (Fig. 6A, E–M). Wiele warstw turbidytów wapiennych zawiera również małe ślady z ichnorodzaju *Chondrites* (Fig. 4B) i *Thalassinoides*. Wszystkie warstwy margli są silnie impregnowane diagenetyczną krzemionką. W obrębie tej sukcesji występują również bardzo cienkie utwory hemipelagiczne, tj. zielone i czarne łupki bezwapniste. Zawierają one zespoły głębokowodnych otwornic aglutynujących z formami należącymi głównie do *Plectorecurvoides* sp. (Fig. 7T), *Recurvoides* sp. (Fig. 7U), *Thalmannammina* spp. (Fig. 7S, V), *Glomospira charoides* (Fig. 7G), *Ammodiscus cretaceus* (Fig. 7F), *Bulbobaculites problematicus* (Fig. 7L), *Gerochammina* spp. (Fig. 7W, Z) i *Trochammina* sp. (Fig. 7N, O). Podrzędnie występują tam otwornice rurkowate (Fig. 7A, B) oraz *Pseudonodosinella parvula* (Fig. 7K), *Hippocrepina depressa* (Fig 7C), *Psammosphaera* sp. (Fig. 7D), *Caudammina ovula* (7E) i *Haplophragmoides* spp. (Fig. 7P, R).

Seria wapnistych turbidytów przechodzi stopniowo ku górze do **hemipelagicznych facji wzbogaconych w materię organiczną i promienice** (Fig. 3). Jest to seria naprzemianległych czarnych i zielonych łupków bezwapnistych z podrzędnymi cienkimi wkładkami bentonitów. Pozycja stratygraficzna tej serii odpowiada poziomowi "Bonarelli", znanemu z wielu sukcesji węglanowych w obrębie Zachodniej Tetydy. Zawartość węgla organicznego (TOC) w czarnych łupkach tej sukcesji wynosi od 3,2 do prawie 8% (Bąk K., 2007b). Zespół otwornic aglutynujących w tych osadach, występujący głównie w zielonych łupkach, jest bardzo nieliczny (ok. 10 okazów w 100 g osadu) i zdominowany przez formy o małych rozmiarach należące do *Recurvoides* sp. Podrzędnie występują tam *Ammodiscus cretaceus*, *Glomospira gordialis* (Fig. 7H), *Glomospirella gaultina* (Fig. 7I), *Haplophragmoides* sp., *Gerochammina* sp., ?*Saccammina* sp., *Trochammina* sp. (Fig. 7M) i spirytyzowane otwornice rurkowate.

Warstwa żelazisto-manganowa o miąższości 1,5–3 cm występuje 8–10 cm powyżej stropu facji organicznych. Jest ona zbudowana z koncentrycznie ułożonych tlenków i wodorotlenków Fe, Mn i Ba (mikrosferuli o budowie pasowej), stanowiących pseudomorfozy po węglanach Fe i Mn (Bąk K., 2007b). Mikrosferule Fe-Mn występują w krzemionkowo-ilastym matriks, zawierającym pojedyncze ziarna kwarcu, muskowitu oraz szkielety promienic. Szczegółowy opis tego horyzontu oraz jego korelacja z analogicznymi utworami w innych profilach Karpat Zewnętrznych zostały przedstawione przez autora w innych pracach (Bąk K., 2006, 2007a, b).

Wyżejległa sukcesja osadów o miąższości ok. 70 cm to **czerwone i zielone łupki krzemionkowo-manganowe**, z licznymi laminami wzbogaconymi w promienice (Fig. 3). W jej stropie leży cienki łupek organiczny, a przykrywa go **drugi poziom żelazisto-manganowy**. Pierwsza czerwona warstwa łupku występuje 5 cm powyżej dolnego horyzontu Fe-Mn. W laminie zielonego łupku, który rozdziela ten pierwszy czerwony horyzont występują bardzo liczne i małe otwornice aglutynujące należące do rodzaju *Gaudryina* sp. albo *Uvigerinammina* sp., a także do ?*Ammodiscus* sp. Oprócz wyżej opisanego zespołu, brak jest otwornic bentosowych w tych osadach. Kolejny zespół został znaleziony dopiero w drugim (wyższym) pakiecie sukcesji pstrych łupków, który występuje w kontakcie tektonicznym z niżejległymi osadami. Seria łupków krzemionkowo-manganowych zawiera natomiast liczne promienice (Fig. 8C–J), które tworzą laminy o miąższości 1–3 mm; część z tych lamin ma charakter utworów hemipelagicznych (Fig. 8A), a część reprezentuje utwory przemyte przez prądy denne (Fig. 8B, K). Drugi poziom Fe-Mn ma podobny skład chemiczny, wewnętrzną strukturę i występuje w tej samej pozycji stratygraficznej jak analogiczne utwory w jednostce śląskiej i podśląskiej (Bąk K., 2006, 2007a, b).

Seria **pstrych łupków ilastych**, zdominowana przez łupki zielone, z cienkimi (< 0,5 mm) przeławiceniami turbidytów o frakcji mułowej i pojedynczymi warstwami czarnych łupków organicznych i bentonitów występuje w najwyższej części badanego profilu. Osady te są stektonizowane, występując w dwóch pakietach (Fig. 3). Seria pstrych łupków jest inkrustowana diagenetycznymi tlenkami i wodorotlenkami Fe-Mn (Fig. 9). Zespół promienic występujący w pstrych łupkach jest lepiej zróżnicowany taksonomicznie, podobnie jak i zespół otwornic aglutynujących, który występuje w drugim pakiecie i zawiera zarówno formy znane z górnocenomańskich facji organicznych (*Recurvoides* sp., Fig. 10A, B; ?*Thalmannammina* sp., Fig. 10C; *Trochammina* sp., Fig. 10D, E; *Glomospira glomerata*, Fig. 10G), jak i formy typowe dla turonu, tj. *Gerochammina* sp. (Fig. 10F), *Bulbobaculites problematicus*, *Ammobaculites* sp. (Fig. 10H), *Uvigerinammina praejankoi* (Fig. 10I) i *U. jankoi* (Fig. 10J).

Analizy składu chemicznego łupków zostały wykorzystane w interpretacji zmian dostawy materiału terygenicznego do dna basenu, a także zmian zawartości tlenu w wodach dennych oraz zmian w produktywności wód powierzchniowych.

Jako **chemiczne wskaźniki dostawy materiału okruchowego** wykorzystano proporcje Al_2O_3 do TiO_2, Al_2O_3 do SiO_2 a także Rb do Al, Ti do Al i Al do (Al+Fe+Mn) (Fig. 11, 12). Graficzne porównanie krzywych opartych na powyższych wskaźnikach wskazuje na: 1) znaczące ograniczenie dostawy materiału terygenicznego w czasie sedymentacji facji organicznych oraz sukcesji łupków krzemionkowo-manganowych pomiędzy dwoma poziomami Fe-Mn; 2) wzrost tempa dostawy materiału terygenicznego w czasie depozycji zielonych łupków w obrębie facji organicznych; 3) najniższe tempo sedymentacji w czasie tworzenia się warstw Fe-Mn; 4) malejący udział ziaren pochodzenia eolicznego w górę profilu; 5) brak zróżnicowania w profilu zawartości najdrobniejszych ziaren pochodzenia fluwialnego; 6) dominację krzemionki pochodzenia organicznego w serii łupków krzemionkowo-manganowych, w przeciwieństwie do serii wyżej- i niżejległych, gdzie SiO_2 pochodzi zarówno z rozpuszczenia ziaren kwarcu jak i szkieletów promienic oraz igieł gąbek.

Źródłem materiału terygenicznego i biogenicznego dla serii turbidytowej był szelf w marginalnej strefie platformy zachodnioeuropejskiej. Zespoły otwornic bentosowych wskazują, że większość materiału pochodziła ze strefy nerytycznej i górnego batiału. Mikrofacje i struktury sedymentacyjne w turbidytach wapiennych wskazują, że materiał biogeniczny i siliciklastyczny był dostarczany przez prądy zawiesinowe o niskiej gęstości i małej prędkości.

Seria turbidytów wapiennych w badanym profilu leży w tej samej pozycji stratygraficznej, co osady o podobnym składzie i genezie w jednostce śląskiej (Rogowce Mikuszowickie). Ich sedymentacja zakończyła się również w tym samym czasie (Bąk M. *et al*., 2005), korelowanym z początkiem eustatycznego wzrostu poziomu morza i jednoczesną ekspansją strefy minimum tlenowego. Wzrost poziomu morza spowodował zmniejszenie, a nawet zatrzymanie sedymentacji w basenie skolskim, czego odzwierciedleniem jest powstanie warstw Fe-Mn i serii łupków krzemionkowo-manganowych. Znaczą one maksimum transgresji.

Warunki natlenienia na dnie były interpretowane zarówno na podstawie wskaźników chemicznych takich jak proporcje U do Th, V do (V+Ni) i As do Al, a także w oparciu o skład zespołów otwornic aglutynujących. Graficzna korelacja krzywych chemicznych wskaźników natlenienia (Fig. 13) wskazuje na: 1) najniższy poziom natlenienia wód dennych (warunki anoksyczne i euksyniczne) w czasie późnocenomańskiej sedymentacji facji organicznych, z fluktuacjami w zawartości tlenu w czasie sedymentacji łupków organicznych i łupków zielonych; 2) wyższy poziom natlenienia wód dennych i porowych w czasie sedymentacji łupków zielonych, potwierdzony obecnością skamieniałości śladowych z ichnorodzaju *Chondrites* oraz zespołu otwornic aglutynujących, należących do tzw. Biofacji "B"; 3) dysoksyczne i anoksyczne warunki na dnie w czasie późnomioceńskiej sedymentacji serii turbidytów wapiennych; 4) znaczną poprawę natlenienia na dnie od zakończenia sedymentacji utworów organicznych, z epizodami warunków anoksycznych.

Powstanie warstw Fe-Mn, pierwotnie jako warstw rodochrozytowych, było związane z inicjalnym etapem zmian w dynamice wód dennych w basenie karpackim. Taki typ osadu powstawał w warunkach dostępności jonów Fe i Mn oraz niedotlenienia wód porowych, które epizodycznie (?cyklicznie) ulegały natlenieniu w wyniku napływu gorących, dobrze natlenionych wód transportowanych przez prądy denne (szczegóły genezy utworów Fe-Mn – Bąk K., 2006). Wskaźnik natlenienia wód dennych (Ce/La; Tab. 1) wskazuje jednak na niewielką prędkość prądów dennych, która wzrastała prawdopodobnie jedynie epizodycznie.

Materia organiczna w czarnych łupkach jest głównie pochodzenia morskiego (Bąk K., 2007b). Jednym z jej źródeł były glony, na co wskazuje wysoka zawartość arsenu w niektórych próbach czarnych łupków.

Zmiany w produktywności wód powierzchniowych były interpretowane w oparciu o wskaźniki chemiczne, tj. proporcje udziału Ba i Al oraz Ba i Sc, przy zachowaniu świadomości o różnych ograniczeniach tej metody w związku z potencjalną możliwością wczesnodiagenetycznego uwolnienia Ba z biogenicznych siarczanów w warunkach anoksycznych panujących w kolumnie wody i na dnie oraz brakiem znajomości wszystkich źródeł pochodzenia baru. Negatywna korelacja pomiędzy wartościami Ba/Al i wskaźnikami natlenienia osadu w obrębie facji organicznych wyklucza możliwość interpretacji produktywności dla tej części profilu. Porównując wartości Ba/Al i Ba/Sc pomiędzy górnocenomańskimi łupkami hemipelagicznymi a dolnoturońskimi łupkami pstrymi można stwierdzić wzrost produktywności wód powierzchniowych we wczesnym turonie. Potwierdza to bardzo wysoka zawartość baru w obrębie warstwy Fe-Mn, porównywalna z wartościami we współczesnych środowiskach o wysokiej produktywności, a także obecność licznych lamin z promienicami w serii łupków krzemionkowo-manganowych. Zespół promienic w obrębie całego badanego profilu jest zdominowany przez małe, ?oportunistyczne formy z rodzaju *Holocryptocanium*, co mogłoby wskazywać na podwyższoną produktywność w basenie w warunkach ?sezonowej cyrkulacji upwelingowej.